# CHAPTER 8

# MODELING AND SIMULATION OF MINIATURE AERIAL VEHICLES

## 8.1 INTRODUCTION

Successful flights with airplanes with no pilot onboard predate the first successful controlled airplane flights in 1903 by the Wright Brothers. In 1896, Samuel Pierpont Langley's team successfully flew a small steam-powered airplane model more than 3/4 of a mile (Anderson, 2008). Significantly, these first aircraft without a pilot onboard, a condition often referred to as *unmanned*, were not controlled. That is, their flight path was neither directed nor predictable. This limited the utility of such an airplane to verify design principles without putting a pilot at risk.

The decades that followed included several notable attempts at making an operationally useful unmanned aircraft. One area of considerable focus was the *cruise missile*. Here, an airplane is launched carrying a bomb that is directed on a one-way flight to a target. The Kettering Bug was developed in the United States and flew in 1918. The German V-1 flying bomb became the first cruise missile used in large numbers in 1944 to 1945, including many strikes directed at Britain. A second area of early usage of unmanned aircraft going on at the same time was as a *target drone*, where an unmanned aircraft was used for target practice or anti-aircraft weapons testing. These types of systems date back to 1935. The newest examples include unmanned variants of manned aircraft, such as a variant of the General Dynamics F-16 referred to as the QF-16.

As the guidance and control capabilities of these aircraft improved, the practical applications of unmanned airplanes expanded beyond the high-risk domains of aeronautics testing, target practice, and cruise missiles. Unmanned aircraft could now be precisely flown and recovered reliably. Communications capabilities also allowed them to be *remotely operated*, enabling real-time commands to be sent to the aircraft

*Aircraft Control and Simulation: Dynamics, Controls Design, and Autonomous Systems, Third Edition.*
Brian L. Stevens, Frank L. Lewis, Eric N. Johnson.

and for the aircraft to send useful data to multiple users. By the 1990s systems such as the General Atomics MQ-1 Predator could be remotely operated via satellite for hours at a time and communicate high-quality video back to its operators. Following the attacks of September 11, 2001, an ongoing debate about the efficacy of using these types of aircraft to actually launch weapons ended. The result was the first systems capable of identifying, following, and then killing individuals from a single unmanned aircraft without putting the operators of the aircraft in harm's way. By many accounts, this was revolution in military affairs, changing the way wars are fought.

Recent decades have seen other areas of successful use of unmanned aircraft. The Yamaha RMAX is a small unmanned helicopter that has been used commercially since 1997 for widespread use in agriculture in Japan and other countries. Other application areas of interest include law enforcement, filmmaking, surveying, scientific research, logistics, and security.

No discussion of the use of small aircraft could be made without mentioning that flying small model aircraft for recreation also goes back to the dawn of aviation. The miniaturization and cost reduction of batteries, sensors, and processors associated with smartphones have led to a dramatic rise in the capabilities of small and inexpensive miniature unmanned aircraft since the mid-2000s. Very small and inexpensive airplanes and vertical take-off and landing (VTOL) aircraft can fly precisely, carry high-definition imagers, and be effectively remotely operated by an operator with limited training. Often first envisioned for recreational users, these types of systems have become good enough for many of the other application areas above. Aerial photography in particular is perhaps the most widespread commercial use of these small systems today.

A particular aircraft configuration that has been enabled by this trend in small electronics is the *multirotor*. This is a VTOL aircraft where several electric motors with propellers are mounted to a frame. Changing the power of the individual motors is used to change the velocity and attitude of the aircraft. When the multirotor specifically has four motors/propellers, it is often referred to as either a *quadrotor* or *quadcopter*; if it has six motors, as a *hexarotor* or *hexacopter*; and if it has eight motors, then as an *octorotor* or *octocopter*. Multirotors with other numbers of motors are also used.

From an aircraft performance standpoint, unmanned aircraft share many common characteristics with manned aircraft. Maximum range and endurance are key performance parameters dictated by the intended missions. Aircraft sizing dictates that a given aircraft design can be scaled larger to increase maximum range and endurance. Due to the energy density of fossil fuels vs. batteries available today, aircraft with very large range or endurance requirements tend to use internal combustion engines that burn fossil fuels. Electric propulsion is common today on aircraft that are very small and do not require long range or endurance. They benefit from the cost, simplicity, and low noise of electric propulsion. Aircraft that utilize solar energy collection are able to break out of this energy storage limitation and are an area of ongoing development.

A key challenge associated with all of these unmanned aircraft systems is achieving a desired level of reliability without a human pilot onboard to

control it. A remotely piloted aircraft relies on pilot inputs arriving via a wireless communication system. Such a system is subject to time delays, bandwidth limitations, and drop-outs that must be accounted for. Many successful systems provide the option of automated flight control and guidance to reduce operator workload and to account for potential loss of communication. Such a system is often described as having a higher degree of *autonomy* or *automation* due to this reduced reliance on the human operator. When flown by the human operator, many systems today also provide enough stability and control augmentation to make the handling qualities good enough that even an inexperienced pilot is able to effectively perform necessary flight maneuvers. So, although many of these miniature aircraft look simple, the underlying control and simulation problems are as complex as any other aircraft.

### Propellers vs. Rotors

Chapters 1 to 3 covered equations of motion and modeling of aircraft. In this chapter, that material is expanded upon for miniature aircraft. The models described for aerodynamic forces and moments apply here as well. For miniature aircraft, one key difference is the lower Reynolds numbers associated with the smaller size. This may imply somewhat different forces and moments for a given aerodynamic shape, but not a change in how we construct our aerodynamic models (Abbot and Von Doenhoff, 1959). Specifically, quantities like dynamic pressure and angle of attack will still be important inputs for our models of aerodynamic forces and moments. In order to effectively perform modeling and simulation of miniature aircraft, some additional topics are included here that relate to small aircraft (e.g., rotorcraft); including modeling propellers, rotors, and motors. This chapter also describes three miniature aircraft models: a small propeller-driven airplane, the Aeroworks 33% Edge 540T; a quadrotor aircraft (example of a multirotor), the AscTec Pelican; and a small helicopter, the Yamaha RMAX.

Typical terminology ascribes the name propeller to a rotating set of angled blades that provide thrust for an airplane. It is common to refer to the similar device on a helicopter or multirotor as a rotor. In this chapter, we will largely keep to this convention. From a modeling perspective, there are actually far more useful distinctions. Table 8.1-1 lists some key distinctions between propeller and rotor classes.

Starting with the fixed-pitch propeller, we see what is probably the simplest class (Figure 8.1-1): a solid object mounted to a shaft with a distinct shape so that it produces thrust when spinning. This is a common choice for propulsion on small airplanes as well as conventional multirotor configurations, including quadrotors. The primary means of increasing the thrust of this type of propeller as a means of control is to add additional power. This will cause the propeller to seek a new higher equilibrium RPM corresponding to a higher thrust and torque. Key characteristics of the fixed-pitch propeller include its diameter, pitch, number of blades, chord, stiffness, and mass properties.

For the multirotor configuration, complete attitude control can be obtained with, for example, four independent body-fixed motors/propellers, as illustrated in Figure 8.1-2 for a quadrotor. Each motor provides both thrust and a significant

**TABLE 8.1-1 Common Propeller and Rotor Classes**

| Name | Description | Typical Uses |
|---|---|---|
| Fixed pitch | A single solid structure for the propeller/rotor, typical materials are wood, plastic, and carbon fiber | Airplane propeller, multirotor/quadrotor rotor |
| Variable pitch | Mechanism that enables the pitch of the blades to be varied in order to change thrust at constant RPM | Airplane propeller, helicopter tail rotor |
| Variable pitch and cyclic control | A mechanism that enables the pitch of the blades to be varied in order to change thrust as well as thrust tilting at constant RPM | Helicopter main rotor |
| Variable pitch and cyclic control with stabilizer bar | A mechanism to enable the pitch of the blades to be varied in order to change thrust as well as thrust tilting at constant RPM; a stabilizer bar to improve handling qualities | Helicopter main rotor |

**Figure 8.1-1** Typical fixed-pitch propeller used for small airplanes and multirotors.

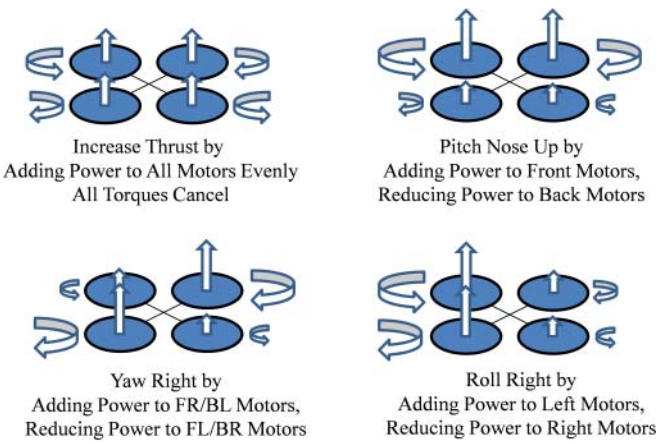


**Figure 8.1-2** A Multirotor with four fixed-pitch propellers (quadrotor) is able to independently control thrust, roll moment, pitch moment, and yaw moment.

reaction torque (corresponding to the lift and drag of the blades). When thrust goes up, so does torque. So, care must be taken to balance these effects when attempting to independently control thrust and individual moments. as shown in the figure. Because these changes in RPM of the individual motors are the primary means of flight control, it is important for multirotor models that the dynamics of propeller RPM be accounted for. Redundancy can be achieved by adding additional motors/propellers. Having an even number of motors allows half to spin in one direction and half to spin in the other, allowing yaw torque to be zero in hover with all motors producing the same thrust by symmetry.

For a helicopter tail rotor, it is typical to mechanically link the tail rotor drive to the main rotor drive. In order to change tail rotor thrust without changing the RPM of the tail rotor (or main rotor), a mechanism to vary the pitch of the blades is typically included, illustrated in Figure 8.1-3. From a modeling perspective, this mechanism is the primary difference between a typical helicopter tail rotor and a fixed-pitch propeller. That is, the propeller can change shape. Larger airplanes often utilize variable-pitch propellers in order to improve efficiency, to allow the blades to be "feathered" in order to minimize drag with a stopped engine, and sometimes to enable reverse thrust. A less common approach for the helicopter tail rotor is to utilize a fixed-pitch propeller with a separate motor to provide an independent control of RPM.

A conventional helicopter obtains primary roll and pitch control by tilting the thrust vector of the main rotor. This is typically accomplished, in conjunction with variable thrust, by adding the capability for the blades to take on different pitch angles as they make each revolution. This is illustrated in Figure 8.1-4. The slider mechanism used for the variable-pitch propeller has been replaced with a *swashplate*. The

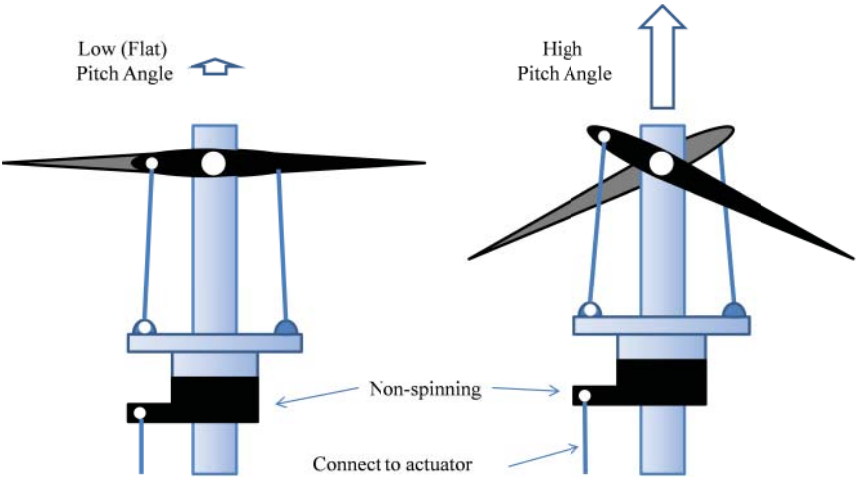


**Figure 8.1-3** Variable-pitch propeller mechanism schematic typical for a small helicopter tail rotor.

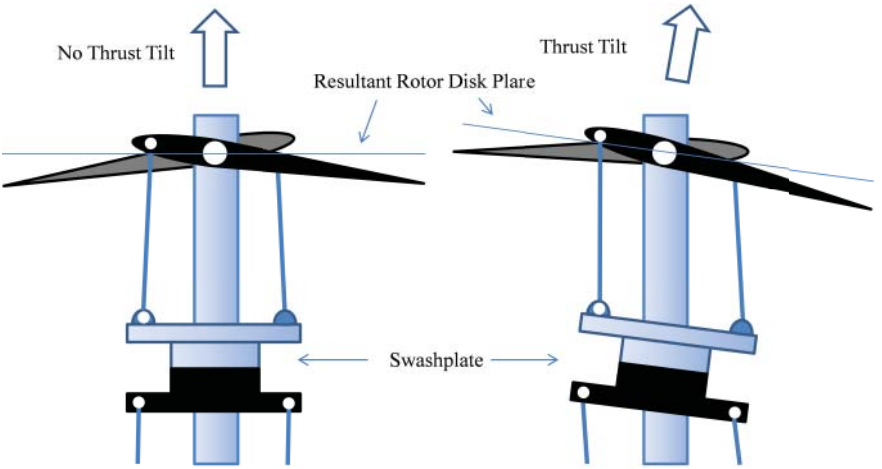


**Figure 8.1-4** Swashplate mechanism schematic typical for a helicopter main rotor.

swashplate has both a rotating and nonrotating element, allowing a transfer of information from the actuators to the rotor blade pitch angle. The swashplate is typically connected to at least three actuators, allowing the plate to both move up/down for variable thrust magnitude as well as tilt the thrust vector fore/aft and left/right. A single direction of tilt is illustrated in Figure 8.1-4. The tilting of the swashplate to the right in the figure causes the blade pitch to be maximum when the blade is pointing out of the page and minimum when it is pointing into the page. This thrust imbalance causes a moment that forces the spinning rotor (effectively a gyroscope) to tilt to the right. The rotor disk becomes tilted relative to the aircraft in a process called rotor flapping. This tilt of the rotor disk plane and the thrust vector generates a moment that can be used to rotate the aircraft. The sections below cover the modeling of these important flapping dynamics, key to describing the motion of helicopters.

Using the swashplate to increase or decrease total thrust by moving it directly up and down along the shaft is called collective pitch. Tilting the swashplate to generate thrust tilt is called cyclic pitch. In general, there are two directions of tilt: roll cyclic (to cause the aircraft to roll) and pitch cyclic (to cause the aircraft to pitch). These three independent actuation channels on the main rotor provide roll, pitch, and thrust control for the conventional helicopter. The tail rotor typically provides the yaw control. These actions are illustrated in Figure 8.1-5.

Some helicopter main rotors also include a stabilizer bar. This is essentially a small "rotor" on the same shaft as the first that exhibits different flapping dynamics than the main rotor, shown in Figure 8.1-6. As discussed below, the stabilizer bar normally responds slower than the main rotor. By mechanically interconnecting the stabilizer bar with the main rotor blade pitch, helicopter handling qualities can be improved by providing a form of feedback to attitude changes. The modeling of such a device can be viewed as an extension of handling main rotor flapping and is covered in this chapter below.

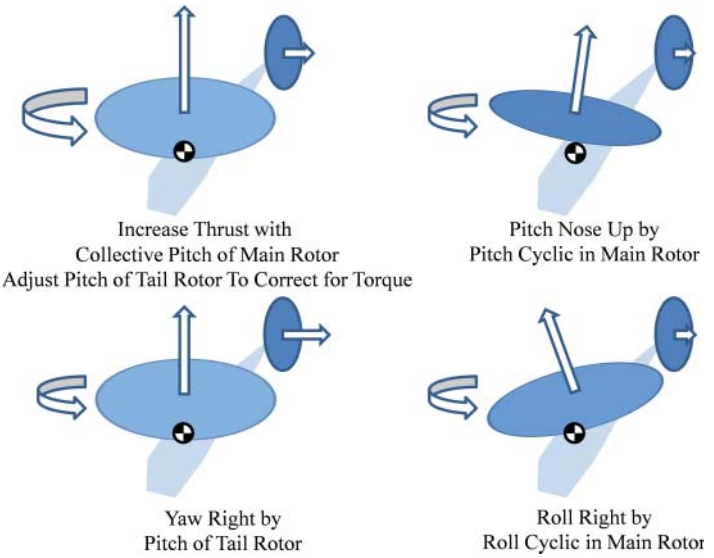


**Figure 8.1-5** A Helicopter is able to independently control thrust, roll moment, pitch moment, and yaw moment via the collective and cyclic pitch of the main rotor and the pitch of the tail rotor.


**Figure 8.1-6** Helicopter main rotor with a stabilizer bar.

Any of these propeller and rotor classes could also be placed inside a duct, creating another distinction to address from a modeling perspective. Properly designed, a true ducted propeller/rotor can have advantages in terms of aerodynamic efficiency. Some of the challenges include getting the flow to enter the duct smoothly, ensuring a small clearance between the propeller tips and the duct wall, and achieving this efficiency benefit across all required flight conditions (McCormick, 1998). Perhaps the most widespread and successful example of this is for helicopter tail rotors, such as seen on the Eurocopter AS365 Dauphin. However, it is still far less common than an unducted tail rotor. Rotor guards placed around the propellers/rotors on successful multirotors are typically there to address possible collisions with obstacles and are sufficiently

small and distant from the rotor itself to avoid the full complexities and efficiency benefits of duct modeling and design.

The sections that follow begin with computing the propeller/rotor forces and moments. This is followed by addressing rotor flapping dynamics. Following that is a discussion of the modeling of gas and electric motors. The chapter concludes with three aircraft model examples chosen to represent one aircraft from each major class of aircraft in common use today. Across the examples, we also see the building blocks for a potentially much larger number of possible aircraft configurations.

## 8.2 PROPELLER/ROTOR FORCES AND MOMENTS

In this subsection, models for the forces and moments due to propellers and rotors are described. One is typically concerned first and foremost with thrust and torque through the propeller shaft, and so this is covered first. An important distinction is made between models that include a degree of freedom (state) for the angular rate of the motor/propeller. For some aircraft, the RPM may be held tightly by a so-called governor or other system. When this is the case, propeller torques are effectively passed through to the aircraft itself. When this is not the case, it may be necessary to explicitly model the RPM or angular velocity of the propeller as it changes. The torques acting on the propeller/rotor are aerodynamic torque, typically opposing rotation, and engine/motor torque, typically causing rotation. The engine torque is imparted on the aircraft in the opposite direction as it applies to the propeller/rotor, as illustrated in Figure 8.2-1, that is, an equal and opposite reaction compared to the propeller/rotor. Because both engine/motor and aerodynamic torques are typically a function of propeller RPM, this model will be fully coupled.

For a fixed-pitch propeller, when an increase in thrust is desired, the pilot might increase the throttle input to the engine/motor. This will cause the engine torque to increase, which will increase the propeller RPM. As RPM climbs, propeller aerodynamic torque will increase until balance is restored. The propeller will now be at a higher RPM corresponding to a higher thrust level. Once RPM is constant again, the aerodynamic torque on the propeller will equal engine torque.

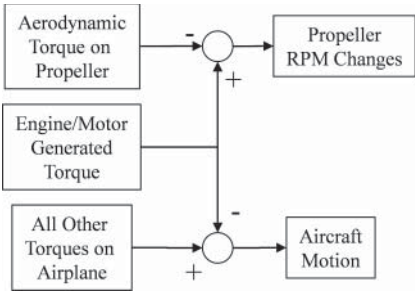


**Figure 8.2-1** Modeling the rotational degree of freedom of a propeller.

The purpose of this section is to provide the tools necessary to model and simulate propellers and rotors in this manner. The level of detail is not sufficient to effectively design and develop propellers or rotor systems, as this is beyond the scope of this book.

A gyrocopter or a helicopter with a power loss represents a case where there is no engine torque into the main rotor, and so the aerodynamic rotor/propeller torques are dominant. So, a gyrocopter in steady flight or a helicopter performing an autorotation can encounter aerodynamic torque that is near zero or even negative by this convention.

### Thrust and Torque of a Propeller/Rotor

Throughout this section we will need to know the local flow properties at the propeller in order to effectively find thrust and torque. It is essential to address the fact that the velocity of the center of a propeller or rotor with respect to the air is not necessarily equal to the velocity of the aircraft itself. It is straightforward to account for the effect of aircraft body angular velocity. This is a dominant effect for helicopter tail rotors and multirotors given their displacement from the center of mass. For propeller $P$, the local velocity relative to the air can be found by

$$\mathbf{v}_{rel}^{P} = \mathbf{v}_{rel}^{bf} + \tilde{\boldsymbol{\omega}}_{b/i}^{bf}\mathbf{p}_{P/CM}^{bf} = \begin{bmatrix} U^P & V^P & W^P \end{bmatrix}^T \tag{8.2-1}$$

$$V_T^P = |\mathbf{v}_{rel}^{P}| \tag{8.2-2}$$

where $\mathbf{p}_{P/CM}^{bf}$ is the location of the propeller with respect to the aircraft center of mass and $\mathbf{v}_{rel}^{bf}$ is the velocity of the aircraft with respect to the surrounding air. The speed of the propeller relative to the air is $V_T^P$. Beyond this correction factor for mounting location, some propellers and rotors are located within the wake or downwash of a wing or another rotor. Of particular concern here is a helicopter tail rotor, where the effect of the main rotor on the flow at the tail rotor can be significant.

A propeller produces thrust by imparting a change in velocity to the air that flows through it. The generated force (thrust) will be in the direction opposite the velocity change imparted on the air flowing through it. For the rotor of a hovering helicopter, this means the still surrounding air will be forced down in order to produce the upward thrust that keeps the helicopter in the air. For the propeller of an airplane in cruise, this means the air goes out the back of the airplane at a speed greater than it arrived at the airplane (from the perspective of an observer in the airplane). Focusing on the latter example, the air of higher speed will take up less area than the air of lower speed to the extent it is at approximately the same density. This effect is illustrated in Figure 8.2-2. In this idealized incompressible flow model, half of the velocity change happens prior to entering the propeller and half occurs after it passes through the propeller. The mass flow rate of the air passing through this propeller is

$$\dot{m} = \rho A(V_T^P + v_i) \tag{8.2-3}$$

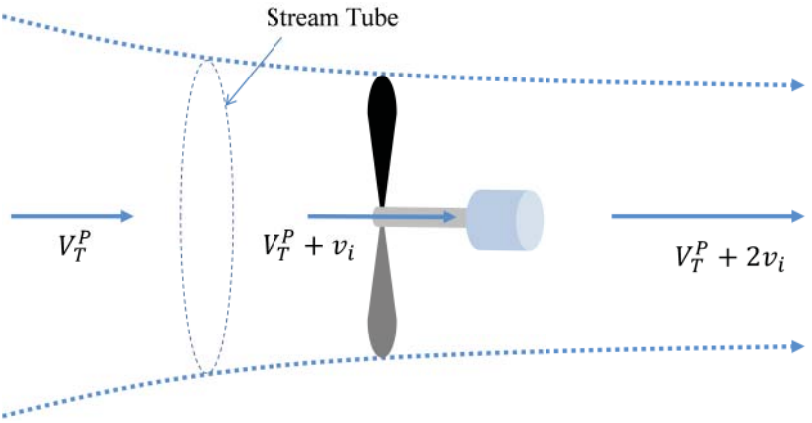


**Figure 8.2-2** Idealized flow through a propeller.

where $A$ is the area of the propeller disk ($A = \pi R^2$). The thrust is mass flow rate multiplied by the total change in velocity caused by the propeller, and is found by

$$T = \dot{m}2v_i = 2\rho A(V_T^P + v_i)v_i \tag{8.2-4}$$

As illustrated in Figure 8.2-2, the induced velocity changes the local flow at the propeller. This will change the effective angle of attack of the propeller blades. Determining propeller thrust, then, is tied to determining this induced velocity and vice versa. We need both a momentum relationship such as Equation (8.2-4) and one that relates thrust to the current angle of attack of the blades, which is itself a function of induced velocity.

Lieshman (2006) has pointed out that for very small rotors in hover the ideal wake contraction shown in Figure 8.2-2 is not fully achieved (perhaps around $R < 8$ inches). This can reduce propulsive efficiency below what is presented here.

However, before we relate blade angle of attack with thrust, we need to deal with the general case where thrust and induced velocity are not aligned with the local flow. This would be the normal case for a helicopter in forward flight. A more general version would be

$$T = \dot{m}2v_i = 2\rho A V' v_i \tag{8.2-5}$$

where the effective speed of the flow at the rotor is

$$V' = \sqrt{U^{P2} + V^{P2} + (W^P - v_i)^2} \tag{8.2-6}$$

for the case where the thrust is directed along the body negative Z-axis, as would be the case for a conventional helicopter, illustrated in Figure 8.2-3 (Stepniewski and Keys, 1984, p. 62).

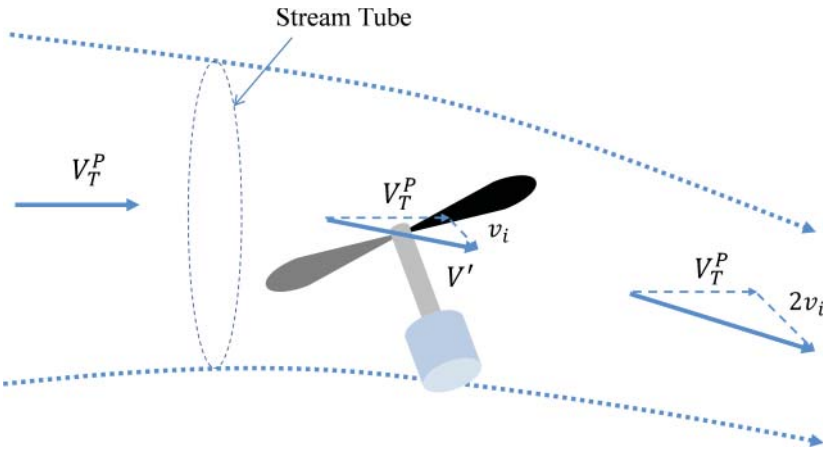


**Figure 8.2-3** Idealized flow through a rotor in forward flight.

The blade element method can be utilized to relate thrust to blade angle of attack and lift properties. Assuming ideal conditions (no blade stall, reverse flow) and a linear blade twist, the local blade angle of attack will be

$$\alpha(\psi, r) = \text{atan}\left(\frac{W^P - v_i}{\Omega r + U^P \sin\psi + V^P \cos\psi}\right) + \theta_0 + \theta_1 \frac{r}{R} \tag{8.2-7}$$

where $\Omega$ is the angular rate of the rotor expressed in radians per second. Here, we are taking care to use $\begin{bmatrix} U^P & V^P & W^P \end{bmatrix}^T$ as the velocity of the propeller/rotor with respect to the air (undisturbed by the rotor itself) expressed in a frame where the rotor thrust is along the negative Z-axis, taking into account rotor disk flapping. Here, $\theta_0$ represents the root blade angle, and $\theta_1$ represents linear twist along the blade. More specifically, this is the angle the zero lift line of the airfoil makes relative to the rotor disk plane (Figure 8.1-4). The angle $\psi$ is the current location of the blade as it travels around a single rotation, zero when pointing straight aft (negative X-axis). We take $r$ to be the blade element location along the blade and $R$ to be the total blade length (Figure 8.2-4).

To get lift per unit span of one blade, one uses

$$\frac{\Delta L(\psi, r)}{\Delta r} = \alpha(\psi, r) a \frac{\rho}{2} (\Omega r + U^P \sin\psi + V^P \cos\psi)^2 c \tag{8.2-8}$$

where $a$ is the lift curve slope of the airfoil and $c$ is the chord of the blade, both assumed constant. To get the total thrust, we integrate the lift along each blade. We integrate again to average that blade for one full rotation. Finally, we multiply by the number of blades ($b$) to get total thrust:

$$T = \frac{b}{2\pi} \int_0^{2\pi} \int_0^R \frac{\Delta L(\psi, r)}{\Delta r} dr d\psi \tag{8.2-9}$$

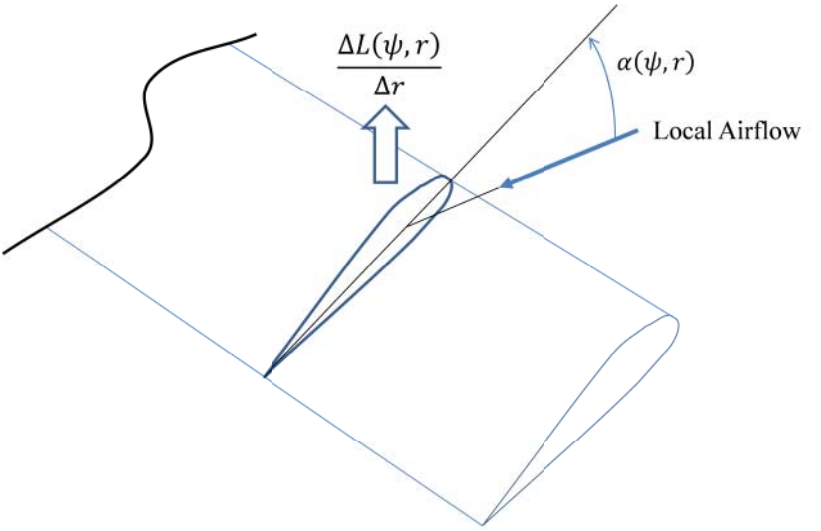


**Figure 8.2-4** Using the blade element method to estimate propeller/rotor thrust.

With these assumptions, it is possible to get a closed-form solution for this integral,

$$T = \frac{\rho abcR}{4}\begin{bmatrix} (W^P - v_i)\Omega R + \frac{2}{3}(\Omega R)^2\left(\theta_0 + \frac{3}{4}\theta_1\right) + \ldots \\ (U^{P2} + V^{P2})\left(\theta_0 + \frac{1}{2}\theta_1\right) \end{bmatrix} \tag{8.2-10}$$

where a small-angle assumption was used to eliminate the atan function in Equation (8.2-7). This blade element method is sufficient for our purposes in this chapter. For a more complete treatment of this topic, including relaxing some of the key assumptions made, see the work of Prouty (1986).

Given the flight condition of the aircraft, the current collective pitch angle (which would be fixed for a fixed-pitch propeller), and rotor/propeller RPM, it is now possible to find the thrust, induced velocity, and flow speed at the propeller by simultaneously solving Equations (8.2-5), (8.2-6), and (8.2-10). A closed-form solution involves finding the roots of a fourth-order polynomial. A common approach is to simply solve it numerically within a simulation model (Figure 8.2-5).

It is also necessary to find the torque exerted by the air on the propeller/rotor. It is convenient to estimate the power first. Following this, one need only divide power by the shaft rate ($\Omega$) to find torque. The first component is the induced power. Note that this contribution can be negative, even with a positive thrust, if the flow is going up through the bottom of the rotor ($W^P > v_i$). It essentially represents the tilt of the lift vector due to the induced velocity:

$$P_{induced} = T(v_i - W^P) \tag{8.2-11}$$

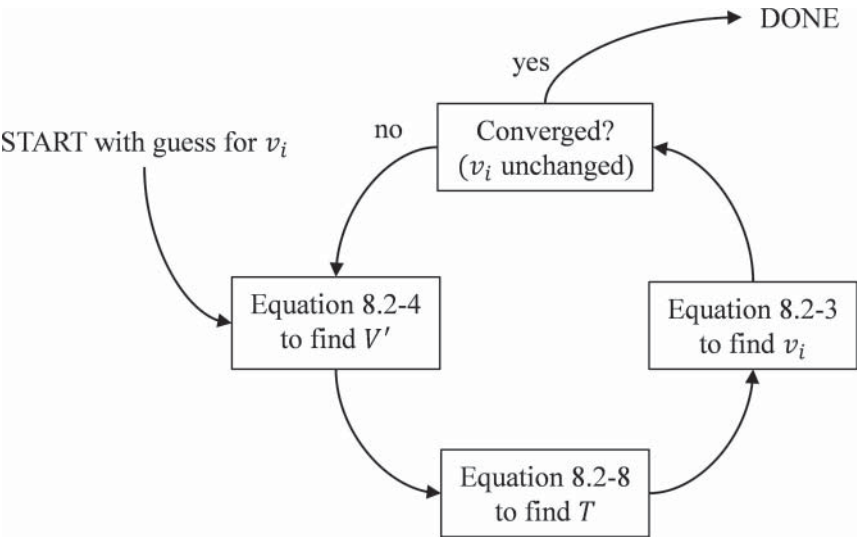


**Figure 8.2-5** Finding rotor thrust and induced velocity numerically.

The second contributor is profile power. This is the skin friction drag of the blades and is positive. This is found in a manner similar to thrust, with more complex versions available that include additional effects. Using the same assumptions we did for thrust (Prouty, 1986; Stepniewski and Keys, 1984, p. 127),

$$P_{profile} = \Omega \frac{b}{2\pi} \int_0^{2\pi} \int_0^R \frac{\Delta D(\psi, r)}{\Delta r} r dr d\psi \tag{8.2-12}$$

$$P_{profile} = \frac{\rho C_{d_0} bc\Omega R^2}{8} \left[ (\Omega R)^2 + U^{P2} + V^{P2} \right] \tag{8.2-13}$$

where $C_{d_0}$ is the zero lift drag coefficient of the blade airfoil. Some sources include a factor of 4.6 on the velocity squared terms, which is effectively a correction factor to account for the effect of forward speed on both profile *and* induced power (Heffley and Mnich, 1987; Stepniewski and Keys, 1984, p. 134), which has already been accounted for here in the profile power directly. We are now ready to compute rotor aerodynamic torque,

$$Q_P = \frac{1}{\Omega} (P_{induced} + P_{profile}) \tag{8.2-14}$$

It is worth noting that we have also calculated the induced velocity of the propeller ($v_i$) in the process of finding thrust and torque. The modeler may find this helpful in determining how the local flow properties have changed for aerodynamic surfaces (or other propellers/rotors) downstream of this propeller/rotor. The total change in the velocity of the flow will be approximately $2v_i$ in a direction opposite to thrust, as

illustrated in Figure 8.2-3. To this level of approximation, the effect would be limited to those areas within the stream tube illustrated in the figure.

These relationships can be utilized to predict the thrust and torque for propellers/rotors mounted on the aircraft in any orientation with an appropriate coordinate transformation. This also includes the case where the direction is time varying due to rotor flapping dynamics or mechanical tilt such as for a tiltrotor aircraft.

An important limitation of the method described here for airplane propellers is the small-angle assumption made for blade angle of attack. This assumption can result in an erroneously large thrust (and low torque) for a typical airplane with a fixed-pitch propeller when the airplane itself is going much slower than the design cruise condition, such as on the ground when starting the takeoff roll. Here, the blade angle of attack may be high enough to result in a loss of lift near the root. To accurately predict thrust and torque for these conditions, such as for takeoff performance analysis, it may be advisable to work with propeller charts that provide thrust and torque coefficients as a nonlinear function of the ratio of blade tip speed to aircraft speed (Phillips, 2010).

***Fixed-Pitch Propeller Nomenclature*** Small propellers/rotors are often specified by two numbers, such as the 9x7 propeller illustrated in Figure 8.1-1. These numbers indicate that the propeller has a diameter of 9 inches and a *pitch* of 7 inches. The pitch is the distance the propeller would travel if "screwed" one revolution. This can be related to the pitch angle of the blade as a function of location along the blade ($r$):

$$\tan[\theta(r)] = \frac{\text{Distance Forward}}{\text{Distance Around}} = \frac{\text{pitch}}{2\pi r} \tag{8.2-15}$$

It is conventional to use $r/R = 0.75$ in Equation (8.2-15) as the point of reference for determining the pitch of the propeller (Simons, 1999):

$$\text{Pitch} = \left(2\pi \tfrac{3}{4}R\right) \tan\left[\theta\left(\tfrac{3}{4}R\right)\right] \tag{8.2-16}$$

To continue with the linear twist assumption utilized in this section, we can approximately match this distribution by enforcing equality of blade pitch at $r/R = 0.75$ and apply the linear twist through that same station:

$$\theta_0 = 2\text{atan}\left(\frac{\text{pitch}}{2\pi \tfrac{3}{4}R}\right), \theta_1 = -\frac{4}{3}\text{atan}\left(\frac{\text{pitch}}{2\pi \tfrac{3}{4}R}\right) \tag{8.2-17}$$

Note that most propellers have cambered airfoils. Thus, the actual collective pitch angle $\theta_0$ is somewhat higher than the airfoil pitch angle to correctly account for the zero-lift angle of attack of the airfoil used.

## Computing Nonthrust Forces and Moments

Although thrust and torque around the prop shaft of a propeller or rotor are usually the dominant forces and moments, the remaining forces and moments can also be

significant. For example, they can cause some of the most important asymmetries for single-engine airplane flight. Here we cover accounting for some of the more important effects.

***Remaining Aerodynamic Forces and Moments*** The most significant remaining force acting on a propeller is that acting perpendicular to thrust within a plane containing both the thrust and the relative velocity vector (Figure 8.2-6). This is the so-called H-force or hub force on a helicopter rotor. For an airplane propeller, it might be called the normal force (normal to thrust).

A closed-form solution can be found for this in a manner similar to thrust and torque. A version with similar assumptions to the thrust and torque relations provided above is

$$H = \frac{b}{2\pi}\int_0^{2\pi}\int_0^R \frac{\Delta D(\psi, r)}{\Delta r}\sin\psi\, dr d\psi \tag{8.2-18}$$

$$H = \frac{\rho C_{d_0} bc\Omega R^2}{4}\sqrt{U^{P2} + V^{P2}} \tag{8.2-19}$$

For an airplane with a propeller, this moment can serve to add or subtract from the static stability (both directionally and longitudinally) depending on whether the propeller is mounted in front of or behind the center of mass (Perkins and Hage, 1949). The effect can be quite pronounced at low speed, given the fact that the moment scales with speed to the first power rather than speed to the second power, as would be the case for a vertical or horizontal fin. The effect can be pronounced even when the propeller is not producing thrust. It only needs to be spinning as found in Equation (8.2-19).

Beyond torque, the remaining aerodynamic moments would only be transferred to the aircraft itself directly for the case of a rigid rotor that is, not when separate flapping dynamics are to be included in the subsection below, where flapping motion is accounted for. When the propeller/rotor is treated as rigid, the moments that would normally cause rotor disk tilt are instead transferred directly to the aircraft itself. For an airplane, the dominant example is a phenomenon called P-factor, where, for example, an aircraft at high angle of attack experiences a yaw moment due to the thrust imbalance between the left and right sides of the propeller disk.

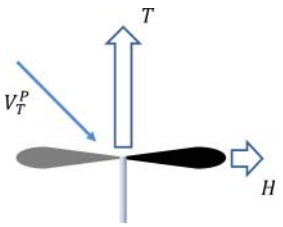


**Figure 8.2-6** H-force acting on a propeller/rotor.

To model these moments, the blade element method can be utilized, this time including the effect of angular velocity of the propeller/rotor:

$$\boldsymbol{\omega}_{P/r}^{P} = \begin{bmatrix} P^P & Q^P & R^P \end{bmatrix}^T \tag{8.2-20}$$

To get a refined estimate for the angle of attack of the blade element,

$$\alpha(\psi, r) = \operatorname{atan}\left(\frac{W^P - v_i + Q^P r\cos\psi + P^P r\sin\psi}{\Omega r + U^P\sin\psi + V^P\cos\psi}\right) + \theta_0 + \theta_1\frac{r}{R} \tag{8.2-21}$$

Using a small-angle assumption to simplify the atan function in Equation (8.2-21), we can find rolling and pitching aerodynamic moments on the propeller/rotor (for a propeller/rotor spinning around the negative $Z$-axis, or counterclockwise as viewed from above):

$$L_{A-P} = -\rho abcR^2\left[\frac{\Omega R^2}{16}P^P + \left(\frac{\left(W^P - v_i\right)}{8} + \frac{\Omega R}{6}\theta_0 + \frac{\Omega R}{8}\theta_1\right)U^P\right] \tag{8.2-22}$$

$$M_{A-P} = -\rho abcR^2\left[\frac{\Omega R^2}{16}Q^P + \left(\frac{\left(W^P - v_i\right)}{8} + \frac{\Omega R}{6}\theta_0 + \frac{\Omega R}{8}\theta_1\right)V^P\right] \tag{8.2-23}$$

Notice that in both cases the propeller/rotor produces a damping effect, where there is a moment-resisting angular rate around that same axis. This is due to the fact any angular velocity will cause a blade lift distribution change that will tend to dampen motion.

For an airplane, the P-factor is predicted by rederiving Equations (8.2-22) and (8.2-23) for the case where the propeller rotor is spinning around the positive $X$-axis (clockwise as viewed from behind), a common choice for an airplane:

$$M_{A-P} = -\rho abcR^2\left[\frac{\Omega R^2}{16}Q^P + \left(\frac{\left(W^P - v_i\right)}{8} + \frac{\Omega R}{6}\theta_0 + \frac{\Omega R}{8}\theta_1\right)V^P\right] \tag{8.2-24}$$

$$N_{A-P} = -\rho abcR^2\left[\frac{\Omega R^2}{16}R^P + \left(\frac{\left(W^P - v_i\right)}{8} + \frac{\Omega R}{6}\theta_0 + \frac{\Omega R}{8}\theta_1\right)W^P\right] \tag{8.2-25}$$

So, if the aircraft is experiencing a large angle of attack, $W^P$ will be large. With typical signs for the remaining parameters (in particular, that thrust is positive), the aircraft will experience a negative yaw moment, $N_{A-P} < 0$.

***Gyroscopic Moments*** If treated as a rigid rotating subsystem, spinning propellers or rotors represent a spinning mass and thus can produce apparent moments. If treated as essentially a separate system with its own attitude motion, as would be the case when including flapping dynamics, then this will be accounted for within

the flapping dynamics themselves. In this section, we address the former case: We want to treat the propeller/rotor as a rigid rotating subsystem.

This is handled by accounting for the angular momentum of the spinning propeller when deriving the rigid-body dynamics of the aircraft. Equation (1.7-3) can be used to find the angular momentum of a rigid body:

$$\mathbf{h}_{cm/i}^{bf} = J^{bf}\boldsymbol{\omega}_{b/i}^{bf}$$

For a rotating subsystem spinning with angular velocity $\boldsymbol{\omega}_{P/b}^{bf}$ and inertia matrix $J_P^{bf}$, the contribution of this subsystem can simply be added, to yield

$$\mathbf{h}_{cm/i}^{bf} = J^{bf}\boldsymbol{\omega}_{b/i}^{bf} + J_P^{bf}\boldsymbol{\omega}_{P/b}^{bf} \tag{8.2-26}$$

with a note that the inertia of the subsystem is included in the original $J^{bf}$ as well. A new version of Equation (1.7-5), the state equation for angular velocity, can be found using this refined term for angular momentum:

$${}^{b}\dot{\boldsymbol{\omega}}_{b/i}^{bf} = (J^{bf})^{-1}\left[\mathbf{M}^{bf} - \tilde{\boldsymbol{\omega}}_{b/i}^{bf}\left(J^{bf}\boldsymbol{\omega}_{b/i}^{bf} + J_P^{bf}\boldsymbol{\omega}_{P/b}^{bf}\right)\right] \tag{8.2-27}$$

Comparing Equations (8.2-27) and (1.7-5), one observes that the effect of the new term is equivalent to a moment, which we will refer to as the *gyroscopic moment*, a name inspired by the observation that this term is critical to the operation of mechanical gyroscopes. So, a good model for the gyroscopic moment of a spinning subsystem is

$$\mathbf{M}_{Gyro-P}^{bf} = -\tilde{\boldsymbol{\omega}}_{b/i}^{bf}J_P^{bf}\boldsymbol{\omega}_{P/b}^{bf} \tag{8.2-28}$$

which is effectively the cross product of the aircraft angular velocity with the angular momentum of the propeller/rotor. So, when an airplane with a single propeller spinning about the longitudinal axis pitches up, it will experience a yawing moment due to this term. The direction depends on the spin direction of the propeller.

This moment can be important for propeller-driven aircraft, particularly those with large propellers. This moment will also be important for multirotors. However, if as many propellers are spinning in one direction as the other, then the effects do tend to cancel each other. If the inertia of the propeller/rotor about the spin axis is the scalar $J_P$ and the propeller/rotor is spinning around the positive body $X$-axis, then

$$\mathbf{M}_{Gyro-P}^{bf} = -\tilde{\boldsymbol{\omega}}_{b/i}^{bf}\begin{bmatrix}J_P\Omega & 0 & 0\end{bmatrix}^T = J_P\Omega\begin{bmatrix}0 & -R & Q\end{bmatrix}^T \tag{8.2-29}$$

It is also worth noting that some aircraft may experience significant gyroscopic moments from rotating parts other that propellers/rotors. Of particular concern may be the effect of the rotating elements of gas turbine engines, which may have a very high angular velocity.

## 8.3 MODELING ROTOR FLAPPING

The motion of a blade as it travels around a helicopter rotor is quite complex. To the extent that the motion is periodic at the frequency of rotor spin when the aircraft is in a steady-state flight condition, it is useful to consider steady (average) conditions separately from what is happening once per revolution, twice per revolution, and so on. If we are particularly concerned with the motion of the aircraft itself, then the average and once-per-revolution conditions typically dominate. Higher-fidelity simulation models would take into account these higher-order harmonics.

### Tip Path Plane Equations of Motion

As introduced in Sction 8.1, the swashplate mechanism can be used to intentionally tilt the rotor disk plane on a helicopter rotor. This has the effect of tilting the thrust vector and is the primary means of attitude control for the aircraft. However, the motion of the aircraft can also change the rotor disk plane tilt. As a result, it is necessary to model the tilt dynamics explicitly. That is, one may need to model the dynamics of the first-order harmonics of blade flapping. The typical symbol for blade flapping is beta, not to be confused with aircraft sideslip angle,

$$\beta(\psi) \cong a_0 - a_1 \cos\psi - b_1 \sin\psi \tag{8.3-1}$$

where $a_0$ represents the coning angle (typically positive), $a_1$ represents longitudinal tilt, and $b_1$ represents lateral tilt, as shown in Figure 8.3-1.

***Coning Angle*** The coning angle ($a_0$) results from a balance between blade thrust load tending to increase the coning angle and centrifugal force tending to reduce it. Coning angle typically responds fast enough to changes in thrust and rotor RPM, so we can simply consider the response to be instantaneous for simulation purposes. An estimate for the opposing moments can be found in the literature (Prouty, 1986) for the case of ideal twist and blades with constant mass distribution. The coning angle is found by setting the sum of these two contributors to the flapping moment to zero,

$$\text{Flapping moment} = 0 = \frac{2}{3}TR - a_0 b I_{Bf} \Omega^2, \tag{8.3-2}$$

where $I_{Bf}$ is the inertia of a single blade around the effective flapping hinge. To solve for the coning angle, one arrives at the approximation

$$a_0 = \frac{2}{3}\frac{TR}{bI_{Bf}\Omega^2} \tag{8.3-3}$$

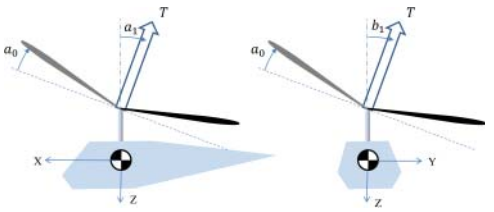


**Figure 8.3-1** Blade first-order harmonic flapping motion (exaggerated).

However, this coning angle will normally not have a significant effect on low-speed motion. Tip path tilt, covered in the next subsection, will.

***Tip Path Tilt*** Unlike the coning angle, the longitudinal and lateral tilt dynamics can couple with the rigid-body motion of the rest of the aircraft. Let us start by estimating the time constant of the response of the rotor if perturbed from an equilibrium tilt angle.

Here we distinguish between a teetering rotor, where the rotor can tilt on a pivot located at the center of rotation, and a rotor where the flapping hinge is offset from the spin axis. The latter case would also approximate a semirigid rotor, where there is a theoretical pivot location that is equivalent to blade behavior as it flexes (Figure 8.3-2).

Prouty (1986, p. 462) found the estimate for rotor flapping time constant in hover as

$$\tau = \frac{16}{\gamma\Omega}\frac{1}{\left(1-\frac{e}{R}\right)^3\left(1+\frac{1}{3}\frac{e}{R}\right)} \tag{8.3-4}$$

Heffley et al. (1986) used a form that matches a Taylor series expansion of the above for small $e$:

$$\tau = \frac{16}{\gamma\Omega}\left(1-\frac{8}{3}\frac{e}{R}\right)^{-1} \tag{8.3-5}$$

Fundamental to this time constant is the value for the Lock number, $\gamma$. This is a nondimensional parameter that characterizes the importance of aerodynamic forces vs. centrifugal forces acting on the blade. It is found by

$$\gamma = \frac{\rho a c R^4}{I_{Bf}} \tag{8.3-6}$$

where $I_{Bf}$ is the blade inertia about the flapping axis rather than the spin axis, normally very nearly the same value as that about the spin axis. A blade with unusually high centrifugal forces, such as one with weights placed in the blade tips, would have a lower Lock number. A rotor with a high Lock number will have a small time constant for flapping motion. That is, it will respond faster.

It is worth noting that some rotor blades will change pitch as they flap, which is the so-called delta-3 effect. Like the hinge offset, this can also lead to a change in the rotor flapping time constant (Dreier, 2007).

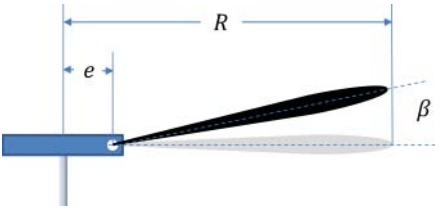


**Figure 8.3-2** Effective hinge offset of a rotor blade.

Now that the time constant of the response has been estimated, we turn to the prediction of the tip path motion, based on Heffley and Mnich (1987) with additional refinements from Mettler (2003):

$$\dot{a}_1 = \frac{1}{\tau}\left(\delta_{pitch} + P\frac{1}{\Omega} + F_c b_1 - F_V U^P - a_1\right) - Q \tag{8.3-7}$$

$$\dot{b}_1 = \frac{1}{\tau}\left(\delta_{roll} - Q\frac{1}{\Omega} - F_c a_1 - F_V V^P - b_1\right) - P \tag{8.3-8}$$

This represents a first-order response around each axis with a time constant for the response found above. The final term represents a direct input to the changes in tilt due to rigid-body motion. For high-speed flight, where the airspeed is greater than perhaps a third of the tip speed ($\Omega R$), it is important to include additional speed effects (Prouty, 1986). The remaining terms deserve detailed discussion, which appears below. In each case a stability or control derivative is introduced with an estimate provided. Values for these sensitivities to motion variables could also be found experimentally. The following subsection extends this model to the case where the rotor has a stabilizer bar.

The $\delta_{pitch}$ and $\delta_{roll}$ terms represent cyclic pitch inputs. When all other terms are small (teetering rotor and no rigid-body motion), then $a_1$ will approach $\delta_{pitch}$, as implied by Figure 8.1-4. Equations (8.3-7) and (8.3-8) imply that the tilt response to a cyclic step input would be exponential with time constant $\tau$ if the aircraft was otherwise constrained not to move.

The $P\frac{1}{\Omega}$ and $Q\frac{1}{\Omega}$ terms are due to the change in the lift distribution of the blades due to vehicle rotation, similar to what was accounted for in the nonflapping rotor by Equations (8.2-22) and (8.2-23). Instead of providing damping, it causes the tip path plane to tilt off axis.

The $F_c$ term, which is zero for a teetering rotor, couples longitudinal and lateral flapping. An estimate provided by Heffley and Mnich (1987) is

$$F_C = \frac{3}{4}\tau\Omega\frac{e}{R} \tag{8.3-9}$$

The $F_V$ term is sometimes referred to as the dihedral effect for a rotor. The moments due to velocity components in the plane of the rotor disk [Equations (8.2-22) and (8.2-23)] are applied to the rotor disk, causing the tip path plane to tilt "away" from the incoming airflow. Based on the sensitivity in hover (Prouty, 1986, p. 564)

$$F_V = \frac{8}{3}\Omega R\left(\theta_0 + \frac{3}{4}\theta_1\right) - 2v_i$$

Rewriting in terms of thrust, as done by Heffley et al. (1986), we obtain the alternate version

$$F_V = \frac{2}{\Omega R}\left(\frac{8T}{\rho abc\Omega^2 R^3} + \sqrt{\frac{T}{2\rho\pi\Omega^2 R^4}}\right) \tag{8.3-10}$$

### Flapping Dynamics with a Stabilizer Bar

As described in Section 8.1, many small helicopters make use of a stabilizer bar (Figure 8.1-6). Our treatment of the flapping dynamics of the main rotor has given us the key necessary tools to model the stabilizer bar.

The stabilizer bar is essentially a second rotor that shares a common shaft with the main rotor. The key difference is that it has much slower flapping dynamics. As the aircraft rotates, the stabilizer bar will lag behind the main rotor. A mechanical interconnect of the stabilizer bar flapping to the cyclic main rotor is then used to create a feedback to resist this attitude displacement.

The typical stabilizer bar is a teetering rotor. So, the flapping time constant can be found, similar to (8.3-5), by

$$\tau_S = \frac{16}{\gamma_S \Omega} \tag{8.3-11}$$

where the Lock number of the stabilizer bar is $\gamma_S$. A complication is that the stabilizer bar is usually not of constant chord. Often it is "paddle" shaped, where the outer section contains a lifting airfoil (Figure 8.3-3). An appropriate relationship to find the Lock number for such a shape is (Mettler, 2003)

$$\gamma_S = \frac{\rho a_S c_S}{I_{Sf}} \left( R_{S,outer}^4 - R_{S,inner}^4 \right) \tag{8.3-12}$$

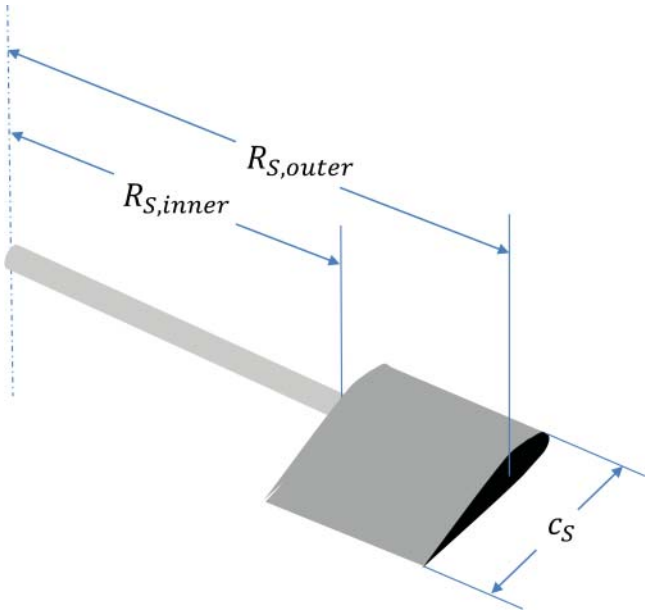


**Figure 8.3-3** Stabilizer bar geometry.

where $a_S$, $c_S$, and $I_{Sf}$ are the lift curve slope, chord, and flapping inertia of the stabilizer bar, respectively, and $R_{S-outer}$ and $R_{S-inner}$ are the outer and inner radii of the lifting section of the paddle. Because of the diminished aerodynamic forces and the common presence of tip weights on the stabilizer bar, this time constant is normally much larger than the main rotor. So, even if the main rotor flapping could be neglected, the dynamics of a well-designed stabilizer bar could not be neglected when modeling aircraft motion.

In order for the stabilizer bar to enhance overall control effectiveness, it is often also given cyclic pitch commands proportional ($K_{C\to S}$) to those sent to the main rotor and in the same manner, that is, via the swashplate. The flapping dynamics of the stabilizer bar can be written as

$$\dot{a}_{1S} = \frac{1}{\tau_S}\left(K_{C\to S}\delta_{pitch} + P\frac{1}{\Omega} - a_{1S}\right) - Q \tag{8.3-13}$$

$$\dot{b}_{1S} = \frac{1}{\tau_S}\left(K_{C\to S}\delta_{roll} - Q\frac{1}{\Omega} - b_{1S}\right) - P \tag{8.3-14}$$

Note that the $\frac{1}{\Omega}$ off-axis terms are typically negligible for a stabilizer bar.

The final step is to modify the main rotor flapping dynamics to account for the presence of the stabilizer bar and the mechanical interconnect of the stabilizer bar flapping to cyclic pitch ($K_{S\to C}$). The revised version has a new term associated with the stabilizer bar interconnect:

$$\dot{a}_1 = \frac{1}{\tau}\left(\delta_{pitch} + K_{S\to C}a_{1S} + P\frac{1}{\Omega} + F_c b_1 - F_V U^P - a_1\right) - Q \tag{8.3-15}$$

$$\dot{b}_1 = \frac{1}{\tau}\left(\delta_{roll} + K_{S\to C}b_{1S} - Q\frac{1}{\Omega} - F_c a_1 - F_V V^P - b_1\right) - P \tag{8.3-16}$$

### Forces and Moments on the Aircraft from a Flapping Rotor

In this subsection, the resultant thrust and flapping angles are utilized to estimate the total forces and moments acting on the aircraft itself. We start with thrust and torque, accounting for the thrust tilt. We must also account for the fact that the rotor is not, in general, mounted at the center of mass. There are also moments that pass through the hub for the nonteetering rotor. Normally, the effect of the stabilizer bar on body forces and moments can be neglected.

If a small-angle assumption is used for the flapping angles, one obtains for a rotor thrusting along the negative $Z$-axis with rotor spinning around the negative $Z$-axis:

$$\mathbf{F}_P^P = \begin{bmatrix} -Ta_1 \\ Tb_1 \\ -T \end{bmatrix} \tag{8.3-17}$$

$$\mathbf{M}_P^P = \begin{bmatrix} -Tz_P b_1 - Ty_P + F_\beta b_1 \\ -Tz_P a_1 + Tx_P + F_\beta a_1 \\ Q_E \end{bmatrix} \tag{8.3-18}$$

where $\begin{bmatrix} x_P & y_P & z_P \end{bmatrix}^T$ is the location of the rotor relative to the aircraft center of mass in the propeller/rotor frame and $Q_E$ is engine torque discussed in the following subsection.

The rotor stiffness $F_\beta$ can be estimated based on the equivalent hinge offset or otherwise determined experimentally. From Prouty (1986, p. 477) we find the commonly used estimate

$$F_\beta = \frac{3}{4} b I_{bf} \Omega^2 \frac{e}{R} \tag{8.3-19}$$

### More Advanced Modeling of Rotors

A variety of phenomena have been neglected in the modeling presented here, including issues such as retreating blade stall, tip and root losses, and more precise models for the shape of the wake. For the purposes of exploring aircraft motion, what we have here is often sufficient for miniature aircraft. For the detailed design of rotor systems, a more advanced treatment is needed; the reader is referred to many of the resources referenced in this chapter, particularly Prouty (1986).

In the modeling included here, we have assumed that the induced velocity will respond instantaneously to changes in the blade geometry and vehicle motion. In reality, it takes a finite amount of time for a real flowfield to adjust. This phenomenon can be important for rotorcraft that are going to be controlled at high bandwidth, particularly larger aircraft. This phenomenon is called dynamic inflow and can be effectively tackled by including an additional state or mode to account for this finite response (Chen and Hindson, 1986).

## 8.4 MOTOR MODELING

Here, we address the issue of modeling a motor or engine to provide power to a propeller or rotor. We limit this to basic/fundamental models suitable to answer questions about the delivery of power and torque within a larger simulation intended to predict aircraft motion, rather than what might be used for motor design.

For small aircraft, the two most common choices for providing mechanical power are the reciprocating internal combustion engine and the electric motor. In both cases, we will predict an engine torque, which will be delivered to the propeller/rotor. At the same time, an equal and opposite moment will go to the aircraft (Figure 8.2-1). With this engine torque computed ($Q_E$), it is then possible to complete our differential equation for propeller/rotor angular rate:

$$\dot{\Omega} = \frac{1}{J_P}(Q_E - Q_P) \tag{8.4-1}$$

where $J_P$ is the moment of inertia (scalar) of the propeller/rotor about its rotation/spin axis. Thus, angular rate $\Omega$ constitutes an additional state to carry along with the rigid-body motion states when performing simulation and analysis.

### Internal Combustion Engine Modeling

The simplest relationship to predict internal combustion engine power is

$$P_E = V_d \frac{\Omega}{2\pi n_p} \overline{p}, \tag{8.4-2}$$

where $V_d$ is the displacement of the engine, $n_p$ is the number of revolutions per power stroke ($n_p = 1$ for a two-stroke engine, $n_p = 2$ for a four-stroke engine), and $\overline{p}$ is the mean effective pressure of the engine (Anderson, 2008). Note that we are continuing to use $\Omega$, or angular velocity of the prop shaft. In many cases, there may be a transmission between the engine and the propeller/rotor, in which case these values would be distinct and related by a gear ratio.

The primary means of controlling engine power for an internal combustion engine is the throttle, which is used to adjust the mean effective pressure between lower and upper limits. When developing a model for simulation purposes, it is typical to have (at best) information about maximum engine power and/or torque as a function of RPM. For a typical engine, one finds that the maximum torque is approximately constant, which means the maximum mean effective pressure is also approximately constant in this case,

$$Q_E = \frac{P_E}{\Omega} = V_d \frac{1}{2\pi n_p} \overline{p} \tag{8.4-3}$$

This suggests that the simplest reasonable model for an internal combustion engine model would be to have it produce a power proportional to throttle (and therefore mean effective pressure) and shaft speed. The effect of density is expected to scale the mean effective pressure as well. The resulting form is

$$P_E(\delta_t, \Omega, \rho) = P_{E,max} \frac{\rho}{\rho_0} \frac{\min(\Omega, \Omega_{max})}{\Omega_{max}} \delta_t, \tag{8.4-4}$$

where $\delta_t$ is the throttle setting with a value between near zero (corresponding to idle) and unity (corresponding to maximum). The angular rate $\Omega_{max}$ corresponds to the RPM of maximum power, and so this term ensures that the engine does not produce power greater than $P_{E-max}$. A more complex model would replace Equation (8.4-3) with lookup tables for maximum power as a function of RPM, for example, as shown in Figure 8.4-1,

$$P_E(\delta_t, \Omega, \rho) = P_{E,max}(\Omega) \frac{\rho}{\rho_0} \delta_t \tag{8.4-5}$$

or even as a lookup table containing up to all three dependencies (density, shaft speed, and density). For a turbocharged engine, this mean effective pressure can be made higher to produce additional power, particularly at high altitude, with power taken from the engine output to generate this additional pressure.

If controlling engine/propeller RPM is of particular interest, then it may be appropriate to also include further dynamics in the response of the engine power found

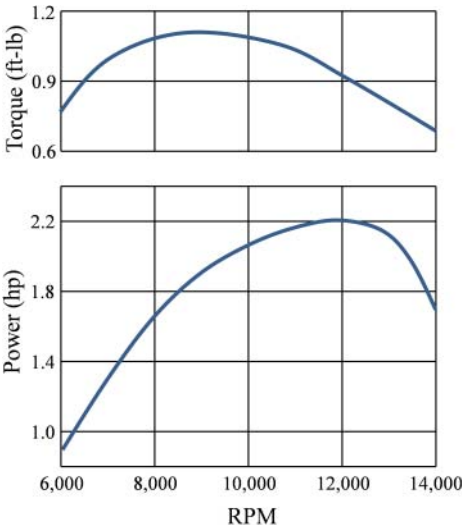


**Figure 8.4-1** Notional engine torque/power curves.

in Equation (8.4-5). These dynamics would normally be associated with mechanical movement of the throttle valve via a servo/actuator.

Fuel consumption can be effectively modeled as proportional to power, using the stated or estimated specific fuel consumption for the engine. That is, amount of fuel used per unit of time per unit of engine power (Anderson, 2008).

### Electric Motor Modeling

Electric motor torque can be effectively modeled as a torque proportional to an input signal and a reduction in torque that comes with increasing RPM (Stingu, 2011), or

$$Q_E(\delta_t, \Omega) = \frac{K_T}{R}\left(\delta_t - \frac{\Omega}{K_V}\right), \tag{8.4-6}$$

where constants $K_T$, $R$, and $K_V$ are properties of the motor (here, $R$ is a resistance paremeter, not to be confused with rotor radius). The input is $\delta_t$, using the same nomenclature as the internal combustion engine above. However, in this case the input would normally be measured in volts.

Modern electronic speed controllers (ESCs) are often used, which will regulate to a desired $\Omega$ or RPM based on the commanded input by adjusting motor torque. The relationship between input and RPM may not be linear and may depend on the input voltage supplied to the ESC from a battery. Because propeller/rotor thrust tends to be proportional to $\Omega^2$, the command $\Omega$ is often proportional to the square root of the input ($\delta_t$) sent to the ESC.

Note that the ESC will achieve the commanded RPM only within the limits of available power and other constraints such as heat dissipation. For the power limit, we would use

$$Q_{E,max}(\Omega) = \frac{1}{\Omega} P_{E,max} \tag{8.4-7}$$

as the relevant torque limit.

## 8.5 SMALL AEROBATIC AIRPLANE MODEL

This subsection contains a medium-fidelity model of a small agile and aerobatic airplane. It is based on the Aeroworks 33% flying scale model of the Zivco Edge 540T, shown in Figure 8.5-1. The aircraft as modeled has been equipped with instrumentation that adds a small amount of weight to the aircraft. Although the aircraft has an outer shape that is a very close match to the full-size aircraft, the mass properties and engine power are not scaled. Unlike the full-scale aircraft, this model has a static-thrust-to-weight ratio greater than unity. Because of the geometry of the propeller prop wash relative to the full-span aileron, elevator, and rudder roll/pitch/yaw control is possible with the aircraft hovering with the nose straight up (Johnson et al., 2008). The aileron authority in hover is marginally enough to counter the torque from the propeller/engine. The example included here contains necessary elements to model this behavior, as well as many other elements of fully aerobatic flight.

The mass properties used for the small airplane example are given in Table 8.5-1. The product-of-inertia terms are assumed to be negligible.

The aerodynamic forces and moments of an airplane can be found using lookup tables. For the intended purpose, the tables need to include the full possible range of angle of attack and sideslip. That type of data is very difficult to obtain, often requiring several types of wind tunnel tests. The approach taken here was to specify the shape of these dependencies and then adjust the parameterization of these curves to match flight data at design conditions corresponding to hover and forward flight. The

**Figure 8.5-1** 33% Zivko Scale Edge 540T made by Aeroworks.

**TABLE 8.5-1 Aeroworks Edge Example Model Parameters: Mass Properties**

| Parameter | Value |
|---|---|
| Weight , mg | 29 lb |
| $X$-axis inertia, $J_x$ | 0.32 slug · ft$^2$ |
| $Y$-axis inertia, $J_y$ | 1.5 slug · ft$^2$ |
| $Z$-axis inertia, $J_z$ | 2.3 slug · ft$^2$ |

net result is a model that should not be considered quantitatively accurate outside of this narrow range yet be considered potentially useful to address basic questions about aircraft motion in these unusual flight conditions. The shape of the dependencies of motion variables will be based on estimating the effect of aircraft components individually and summing them, similar to that described by Dreier (2007).

To account for local flow differences, the effective velocity of each wing (left vs. right) with respect to the local airflow is estimated separately. Note that a term is included to account for the effect of the propeller. For the right wing, this is

$$\mathbf{v}_{rel,rw}^{bf} = \begin{bmatrix} U^{rw} \\ V^{rw} \\ W^{rw} \end{bmatrix} = \begin{bmatrix} U + Qz_{rw} - Ry_{rw} + \eta_w v_i \\ V + Rx_{rw} - Pz_{rw} \\ W + Py_{rw} - Qx_{rw} \end{bmatrix} \tag{8.5-1}$$

where $\eta_w$ is a coefficient that accounts for the level of emersion of the wing in the propeller wash. The position vector $\begin{bmatrix} x_{rw} & y_{rw} & z_{rw} \end{bmatrix}^T$ is chosen to be approximately at the aerodynamic center of the wing panel. A similar velocity is found for the left wing.

The lift and drag of each wing panel are found separately. Continuing to use the right wing to illustrate the approach, the effective dynamic of the right wing is

$$\overline{q}'_{rw} = \frac{\rho}{2}(U^{rw2} + W^{rw2}) \tag{8.5-2}$$

Note that the lateral component $U^{rw}$ has been remitted to approximately account for the effect of sideslip on the lift and drag forces to be calculated using this term. The prime included in the nomenclature is there to remind us of this. The angle of attack is next,

$$\alpha_{rw} = \text{atan2}(W^{rw}, U^{rw}) + \tau_a \delta_a \tag{8.5-3}$$

$$\alpha_{lw} = \text{atan2}(W^{lw}, U^{lw}) - \tau_a \delta_a, \tag{8.5-4}$$

where atan2$(\cdot,\cdot)$ represents a four-quadrant inverse so that $\alpha_{rw}$ can have the full range $-\pi$ to $+\pi$. Note the inclusion of the effect of the aileron here. It modifies the effective angle of attack (with opposite sign for the left wing). The lift coefficient dependency on this angle of attack is found by first checking

$$C_{Lrw}(\alpha_{rw}) = a_w \alpha_{rw} + C_{L0,w} \tag{8.5-5}$$

to determine if it is in the linear range. The linear range is where

$$C_{Lmin,w} < C_{Lrw}(\alpha_{rw}) < C_{Lmax,w} \tag{8.5-6}$$

From the minimum and maximum lift coefficient points, linear interpolation is taken to be $\alpha_{rw} = \pm\pi/2$ and $C_{Lrw} = 0$. This will cause the lift coefficient to fall to zero when the flow is normal to the plane of the wing. Over these same angle-of-attack ranges, a separation drag coefficient ($C_{D,sep}$) is interpolated from zero to a flat-plate drag coefficient for the wing at $\alpha_{rw} = \pm\pi/2$. Rearward flight, corresponding to $|\alpha_{rw}| > \pi/2$, is approximated by

$$C_{Lrw}(\alpha_{rw}) = C_{Dfp,w}\sin(2\alpha_{rw}) \tag{8.5-7}$$

$$C_{D,sep_{rw}}(\alpha_{rw}) = C_{Dfp,w}\frac{1}{2}[1 - \cos(2\alpha_{rw})] \tag{8.5-8}$$

The drag coefficient consists of the separation drag as well as the profile and induced drag,

$$C_{D,sep_{rw}} = C_{D_{0,w}} + k_w\frac{1}{2}C_{L_{rw}}^2 + C_{D,sep_{rw}}(\alpha_{rw}), \tag{8.5-9}$$

where $C_{D_{0,w}}$ is the zero lift drag coefficient of the wing and $k_w$ is the induced drag coefficient. Because of the way they are subsequently dimensionalized, whole airplane parameters can be used here. We take the pitching moment coefficient to be zero for the symmetric airfoil used.

Forces and moments due to the wings can now be computed. Continuing with using the right wing as our example, the dimensionalized lift and drag are found by

$$L_{rw} = C_{Lrw}\frac{S}{2}\overline{q}'_{rw} \tag{8.5-10}$$

$$D_{rw} = C_{Drw}\frac{S}{2}\overline{q}'_{rw}, \tag{8.5-11}$$

where $S$ is the *total* reference wing area. It is important to resolve these into the body axes separately for each wing, as they could potentially be at very different angles of attack,

$$\mathbf{F}_{A,rw}^{bf} = \begin{bmatrix} X_{rw} \\ Y_{rw} \\ Z_{rw} \end{bmatrix} = \begin{bmatrix} +L_{rw}\sin\left(\alpha_{rw}\right) - D_{rw}\cos(\alpha_{rw}) \\ 0 \\ -L_{rw}\cos(\alpha_{rw}) - D_{rw}\sin(\alpha_{rw}) \end{bmatrix} \tag{8.5-12}$$

$$\mathbf{M}_{A,rw}^{bf} = \begin{bmatrix} L_{rw} \\ M_{rw} \\ N_{rw} \end{bmatrix} = \begin{bmatrix} y_{rw}Z_{rw} \\ -x_{rw}Z_{rw} + z_{rw}X_{rw} \\ -y_{rw}X_{rw} \end{bmatrix} \tag{8.5-13}$$

The parameters used for the wing are included in Table 8.5-2.

The horizontal tail is handled as a single panel with lift and drag. First the local velocity is found,

$$\mathbf{v}_{rel,ht}^{bf} = \begin{bmatrix} U^{ht} \\ V^{ht} \\ W^{ht} \end{bmatrix} = \begin{bmatrix} U + Qz_{ht} + \eta_{ht}v_i \\ V + Rx_{ht} - Pz_{ht} \\ W - Qx_{ht} - \eta_{w\to ht}v_{i,w} \end{bmatrix}, \tag{8.5-14}$$

**TABLE 8.5-2 Aeroworks Edge Example Model Parameters: Wing**

| Parameter | Value |
|---|---|
| Wing area, $S$ | 13.0 ft$^2$ |
| Lift-curve slope, $a_w$ | 4.6 |
| Lift coefficient at zero angle of attack, $C_{L0,w}$ | 0 |
| Maximum lift coefficient, $C_{L_{max,w}}$ | 1.1 |
| Minimum lift coefficient, $C_{L_{min,w}}$ | −1.1 |
| Zero lift drag coefficient of wing, $C_{D_{0,w}}$ | 0.01 |
| Induced drag coefficient of wing, $k_w$ | 0.060 |
| Drag coefficient at $\alpha = 90^o$, $C_{D_{fp,w}}$ | 1 |
| Aileron deflection, $\delta_a$ | −0.44 to 0.44 |
| Flap effectiveness of ailerons, $\tau_a$ | 0.4 |
| Effect of prop wash on wing, $\eta_w$ | 0.3 |
| Effective center, body $X$-direction, $x_w$ | 0.2 ft |
| Effective center, body $Y$-direction, $y_w$ | 2.0 ft |
| Effective center, body $Z$-direction, $z_w$ | 0 ft |

where we have once again included a factor for prop wash. This time there is also the potential for downwash from the wing when $U^{ht} > 0$, approximated by estimating the induced velocity of the wing at the wing,

$$v_{i,w} = \max(0, U^h)\frac{1}{2}(C_{L_{rw}} + C_{L_{lw}})k_w \tag{8.5-15}$$

and $\eta_{w\to ht}$ adjusts for the location of the tail within the wing downwash. If fully immersed in the downwash, then the theoretical value would be 2. Effective dynamic pressure and angle of attack for the horizontal tail are given as

$$\overline{q}'_{ht} = \frac{\rho}{2}\left(U^{ht2} + W^{ht2}\right) \tag{8.5-16}$$

$$\alpha_{ht} = \text{atan2}(W^{ht}, U^{ht}) + \tau_e\delta_e \tag{8.5-17}$$

Lift and drag of the horizontal tail are handled in the same manner as for the wing, with different parameter choices. The parameters utilized are given in Table 8.5-3.

The vertical tail is handled very much like the horizontal tail, with the exception of velocity, dynamic pressure, and angle of attack. The vertical-tail angle of attack comes from sideslip of the aircraft:

$$\mathbf{v}^{bf}_{rel,vt} = \begin{bmatrix} U^{vt} \\ V^{vt} \\ W^{vt} \end{bmatrix} = \begin{bmatrix} U + Qz_{vt} + \eta_{vt}v_i \\ V + Rx_{vt} - Pz_{vt} \\ W - Qx_{vt} \end{bmatrix} \tag{8.5-18}$$

$$\overline{q}'_{vt} = \frac{\rho}{2}\left(U^{vt2} + V^{vt2}\right) \tag{8.5-19}$$

$$\alpha_{vt} = \text{atan2}(V^{vt}, U^{vt}) + \tau_r\delta_r \tag{8.5-20}$$

The parameters utilized for the vertical tail are given in Table 8.5-4.

**TABLE 8.5-3 Aeroworks Edge Example Model Parameters: Horizontal Tail**

| Parameter | Value |
|---|---|
| Area, $S_{ht}$ | 3.0 ft$^2$ |
| Lift-curve slope, $a_{ht}$ | 3.6 |
| Lift coefficient at zero angle of attack, $C_{L_{0,ht}}$ | 0 |
| Maximum lift coefficient, $C_{L_{max,ht}}$ | 1.1 |
| Minimum lift coefficient, $C_{L_{min,ht}}$ | −1.1 |
| Zero lift drag coefficient, $C_{D_{0,ht}}$ | 0.01 |
| Induced drag coefficient, $k_{ht}$ | 0.080 |
| Drag coefficient at $\alpha_{ht} = 90^o$, $C_{Dfp,ht}$ | 1 |
| Elevator deflection, $\delta_e$ | −0.30 to 0.30 |
| Flap effectiveness of elevator, $\tau_e$ | 0.5 |
| Effect of prop wash on horizontal tail, $\eta_{ht}$ | 1.6 |
| Effect of wing downwash wash on tail, $\eta_{w\rightarrow ht}$ | 2.0 |
| Effective center, body $X$-direction, $x_{ht}$ | −3.5 ft |
| Effective center, body $Z$-direction, $z_{ht}$ | 0 ft |

**TABLE 8.5-4 Aeroworks Edge Example Model Parameters: Vertical Tail**

| Parameter | Value |
|---|---|
| Area, $S_{vt}$ | 1.3 ft$^2$ |
| Lift-curve slope, $a_{vt}$ | 2.5 |
| Lift coefficient at zero angle of attack, $C_{L_{0,vt}}$ | 0 |
| Maximum lift coefficient, $C_{L_{max,vt}}$ | 1.1 |
| Minimum lift coefficient, $C_{L_{min,vt}}$ | −1.1 |
| Zero lift drag coefficient, $C_{D_{0,vt}}$ | 0.01 |
| Induced drag coefficient, $k_{vt}$ | 0.084 |
| Drag coefficient at $\alpha_{vt} = 90^o$, $C_{Dfp,vt}$ | 1 |
| Rudder deflection, $\delta_r$ | −0.50 to 0.50 |
| Flap effectiveness of rudder, $\tau_r$ | 0.7 |
| Effect of prop wash on vertical tail, $\eta_{vt}$ | 1.6 |
| Effective center, body $X$-direction, $x_{vt}$ | −4.1 ft |
| Effective center, body $Z$-direction, $z_{vt}$ | −0.60 ft |

The aerodynamic forces and moments of the fuselage are approximated in a manner similar to that used by Heffley and Mnich (1987) for a helicopter. This method is described in greater detail below in Section 8.7 for the helicopter example. Here, it is just capturing the drag of the fuselage. Using this approach, fuselage aerodynamic force is found by

$$\mathbf{F}^{bf}_{A,\,fuse} = \begin{bmatrix} X_{fuse} \\ Y_{fuse} \\ Z_{fuse} \end{bmatrix} = -\frac{\rho}{2} \begin{bmatrix} X_{fuse,uu} \left|U + 2v_i\right| (U + 2v_i) \\ Y_{fuse,vv} |V| V \\ Z_{fuse,ww} |W| W \end{bmatrix}, \tag{8.5-21}$$

where $X_{fuse,uu}$, $Y_{fuse,vv}$, and $Z_{fuse,ww}$ are appropriate dimensional coefficients for each basis functions, and they are given in Table 8.5-5 for the example airplane. As formulated, they are the equivalent flat-plate area for flow in each of the three basis directions. Note that the local flow effect of the propeller, in this case assumed to be located well behind the propeller, is approximated. The corresponding moment is estimated by

$$\mathbf{M}_{A,fuse}^{bf} = \begin{bmatrix} L_{fuse} \\ M_{fuse} \\ N_{fuse} \end{bmatrix} = \begin{bmatrix} -z_{fuse} Y_{fuse} \\ -x_{fuse} Z_{fuse} + z_{fuse} X_{fuse} \\ x_{fuse} Y_{fuse} \end{bmatrix}, \tag{8.5-22}$$

where $x_{fuse}$, $z_{fuse}$ is the effective center of the fuselage expressed in the body frame.

The aircraft is equipped with a fixed-pitch propeller and a two-stroke internal combustion engine. The parameters for this combination are listed in Table 8.5-6. The propeller spins clockwise as viewed from behind. Gyroscopic torques can also be computed using the parameters included here.

**TABLE 8.5-5 Aeroworks Edge Example Model Parameters: Fuselage**

| Parameter | Value |
|---|---|
| $X$-axis force coefficient, $X_{fuse,uu}$ | 0.15 ft$^2$ |
| $Y$-axis force coefficient, $Y_{fuse,vv}$ | 1.2 ft$^2$ |
| $Z$-axis force coefficient, $Y_{fuse,ww}$ | 1.0 ft$^2$ |
| Effective center, body $X$-direction, $x_{fuse}$ | −1.5 ft |
| Effective center, body $Z$-direction, $z_{fuse}$ | 0 ft |

**TABLE 8.5-6 Aeroworks Edge Example Model Parameters: Engine and Propeller**

| Parameter | Value |
|---|---|
| **Engine** | |
| Maximum power, $P_{E,max}$ | 90% of rated 9.8 hp |
| Engine speed at best power, $\Omega_{max}$ | 1000 rad/s |
| **Propeller** | |
| Radius, $R$ | 1.1 ft |
| Lift-curve slope, $a$ | 5.9 |
| Number of blades, $b$ | 2 |
| Blade effective chord, $c$ | 0.17 ft |
| Effective zero lift drag coefficient, $C_{d_0}$ | 0.01 |
| Root blade pitch, $\theta_0$ | 0.31 |
| Blade twist, $\theta_1$ | −0.21 |
| Inertia of rotor about spin axis, $J_P$ | 0.0020 slug · ft$^2$ |
| Location, body $X$-direction, $x_P$ | 2.2 ft |
| Location, body $Z$-direction, $z_P$ | 0 ft |

## 8.6 QUADROTOR MODEL

This subsection contains a medium-fidelity model of a quadrotor, or multirotor with four rotors. It represents a configuration of the AscTec Pelican aircraft, which is typically modified heavily for research purposes. The aircraft is shown in Figure 8.6-1 as utilized at the Georgia Institute of Technology for navigation research (Chowdhary et al., 2011).

The mass properties used for the multirotor example are given in Table 8.6-1. The product-of-inertia terms are assumed to be negligible.

The four rotors are treated as rigid, each with independent speed control. The rotors, speed controllers, and motors are identical, with the exception that two spin clockwise as viewed from above and two counterclockwise. The parameters are listed in Table 8.6-2 for the rotors.

The combination of the motor and electronic speed controller was modeled as a first-order system for rotor angular velocity. Here, we assume the speed controller is aggressively tracking the desired angular speed command $\sqrt{\delta_t}$. This would correspond to a motor torque of

$$Q_E(\delta_t, \Omega) = \min\left[J_P\left(\sqrt{\delta_t} - \Omega\right)\frac{1}{\tau_{ESC}} + Q_P, \frac{1}{\Omega}P_{E,max}\right], \tag{8.6-1}$$

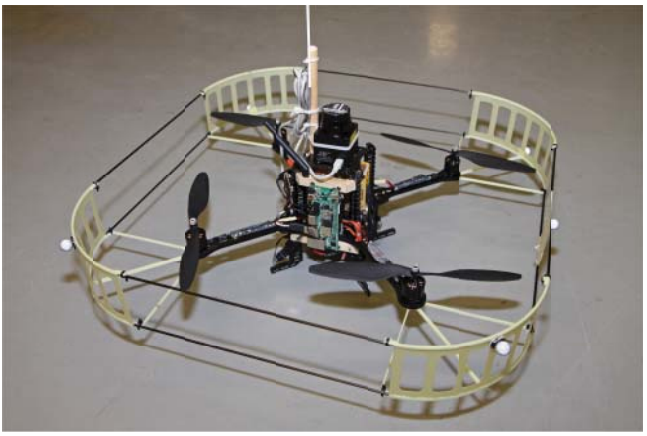

**Figure 8.6-1** Modified AscTec Pelican Quadrotor as configured at the Georgia Institute of Technology.

**TABLE 8.6-1 AscTec Pelican Example Model Parameters: Mass Properties**

| Parameter | Value |
|---|---|
| Weight, $mg$ | 2.8 lb |
| $X$-axis Inertia, $J_x$ | 0.032 slug · ft$^2$ |
| $Y$-axis Inertia, $J_y$ | 0.032 slug · ft$^2$ |
| $Z$-axis Inertia, $J_z$ | 0.052 slug · ft$^2$ |

**TABLE 8.6-2 AscTec Pelican Example Model Parameters: Rotor (each)**

| Parameter | Value |
|---|---|
| Radius, $R$ | 0.42 ft |
| Lift-curve slope, $a$ | 5.7 |
| Number of blades, $b$ | 2 |
| Blade effective chord, $c$ | 0.09 ft |
| Effective zero lift drag coefficient, $C_{d_0}$ | 0.01 |
| Root blade pitch, $\theta_0$ | 0.49 |
| Blade twist, $\theta_1$ | −0.33 |
| Inertia of rotor about spin axis, $J_P$ | 0.000030 slug · ft$^2$ |
| Location, body $X$-direction, $x_P$ | ±0.49 ft |
| Location, body $Y$-direction, $y_P$ | ±0.49 ft |
| Location, body $Z$-direction, $z_P$ | 0 ft |

**TABLE 8.6-3 AscTec Pelican Example Model Parameters: Motor and Speed Control (each)**

| Parameter | Value |
|---|---|
| Maximum power, $P_{E,max}$ | 0.21 hp |
| Time constant for electronic speed control, $\tau_{ESC}$ | 0.05 s |

which results in a first-order lag for angular speed tracking (if torque does not hit power limit) of the form

$$\dot{\Omega} = \left(\sqrt{\delta_t} - \Omega\right) \frac{1}{\tau_{ESC}} \tag{8.6-2}$$

The parameters used are listed in Table 8.6-3. In practice, the propeller/rotor torque $Q_P$ in Equation (8.6-1) would come from the integration of tracking error within the speed controller. Because thrust tends to be proportional to $\Omega^2$ rather than $\Omega$, this nonlinearity is approximately accounted for by viewing $\delta_t$ as the square of commanded angular speed. This is also handled by the speed controller.

## 8.7 SMALL HELICOPTER MODEL

This subsection contains a medium-fidelity model of a small helicopter based on a configuration of the Yamaha RMAX aircraft. It was specifically configured at the Georgia Institute of Technology as a research aircraft (Johnson and Schrage, 2004). This included the addition of instrumentation and processing capabilities. The aircraft is shown in Figure 8.7-1. The aircraft is primarily intended for agricultural applications. Simulation results utilizing this model are included in Section 9.5.

The mass properties used for the example are given in Table 8.7-1. The product-of-inertia terms are assumed to be negligible.


**Figure 8.7-1** Yamaha RMAX as configured at the George Institute of Technology.

**TABLE 8.7-1 Yamaha RMAX Example Model Parameters: Mass Properties**

| Parameter | Value |
|---|---|
| Weight, $mg$ | 166 lb |
| $X$-axis Inertia, $J_x$ | 2.3 slug · ft$^2$ |
| $Y$-axis Inertia, $J_y$ | 8.3 slug · ft$^2$ |
| $Z$-axis Inertia, $J_z$ | 7.3 slug · ft$^2$ |

The main rotor is modeled with first-order flapping dynamics with a nonzero effective hinge offset. The parameters for this main rotor with stabilizer bar are given in Table 8.7-2. Note that this rotor spins clockwise as viewed from above.

The tail rotor is modeled as rigid, with parameters given in Table 8.7-3. Note the necessity to adapt the thrust calculations for the case where the rotor is pointed along the body $Y$-axis. The thrust is defined as positive to the left in this case, due to the clockwise spinning rotor. By making this choice, tail rotor thrust is normally positive. As is common for small helicopters, the yaw handling qualities are improved by providing a rate feedback to augment the tail rotor pitch command. Here, this is modeled with

$$\theta_{0,augmented} = \theta_0 - K_{SAS}R, \tag{8.7-1}$$

where $R$ is the measured body-fixed axis yaw angular velocity and $K_{SAS}$ is the fixed feedback gain.

**TABLE 8.7-2 Yamaha RMAX Example Model Parameters: Main Rotor**

| Parameter | Value |
|---|---|
| **Main Rotor** | |
| Radius, $R$ | 5.1 ft |
| Normal rotor speed, $\Omega$ | 90 rad/s |
| Lift-curve slope, $a$ | 5.7 |
| Number of blades, $b$ | 2 |
| Blade effective chord, $c$ | 0.43 ft |
| Effective hinge offset, $e$ | 0.2 ft |
| Effective Inertia of a blade about flapping hinge, $I_{Bf}$ | 1.0 slug $\cdot$ ft$^2$ |
| Inertia of complete rotor system about spin axis, $J_P$ | 2.0 slug $\cdot$ ft$^2$ |
| Effective zero lift drag coefficient, $C_{d_0}$ | 0.01 |
| Root blade pitch (collective) of zero lift line, $\theta_0$ | 0.12 to 0.30 |
| Blade twist, $\theta_1$ | $-0.1$ |
| Cyclic pitch, $\delta_{pitch}$ or $\delta_{roll}$ | $-0.12$ to 0.12 |
| Location, body $X$-direction, $x_{P,mr}$ | 0 ft |
| Location, body $Z$-direction, $z_{P,mr}$ | $-1.4$ ft |
| **Main Rotor Stabilizer Bar** | |
| Outer radius of paddle, $R_{S,outer}$ | 2.1 ft |
| Inner radius of paddle, $R_{S,inner}$ | 1.5 ft |
| Lift-curve slope, $a_S$ | 2.8 |
| Blade effective chord, $c_S$ | 0.35 ft |
| Effective Inertia of a blade about flapping hinge, $I_{Sf}$ | 0.24 slug $\cdot$ ft$^2$ |
| Cyclic pitch of stabilizer bar per cyclic pitch to main rotor, $K_{C\to S}$ | 4.5 |
| Cyclic pitch of main rotor per flap of the stabilizer bar, $K_{S\to C}$ | 0.33 |

**TABLE 8.7-3 Yamaha RMAX Example Model Parameters: Tail Rotor**

| Parameter | Value |
|---|---|
| Radius, $R$ | 0.69 ft |
| Lift-curve slope, $a$ | 5.0 |
| Number of blades, $b$ | 2 |
| Blade effective chord, $c$ | 0.15 ft |
| Effective zero lift drag coefficient, $C_{d_0}$ | 0.01 |
| Root blade pitch, $\theta_0$ | 0.0 to 0.30 |
| Blade twist, $\theta_1$ | 0 |
| Stability augmentation system gain, $K_{SAS}$ | 0.06 s |
| Location, body $X$-direction, $x_{P,tr}$ | $-6.04$ ft |
| Location, body $Z$-direction, $z_{P,tr}$ | $-0.47$ ft |

**TABLE 8.7-4 Yamaha RMAX Example Model Parameters: Engine and Transmission**

| Parameter | Value |
|---|---|
| Maximum power, $P_{E,max}$ | 90% of rated 21 hp |
| Engine speed at best power, $\Omega_{max}$ | 680 rad/s |
| Engine RPM per main rotor RPM | 7.55 : 1 |
| Tail rotor RPM per main rotor RPM | 6.71 : 1 |

The aerodynamic forces and moments of the tail and fuselage can be modeled in the same manner as an airplane tail and fuselage. However, it is clearly important to include sideways and rearward flight. So, if lookup tables are to be used, then they need to include the full possible range of angle of attack and sideslip. To the extent that rotor forces and moments are expected to dominate, an appropriate medium-fidelity approach is used, inspired by Heffley and Mnich (1987), which utilizes appropriate nonlinear basis functions. It is interesting to note that this is also a common approach to model airship or submarine hulls (Feldman, 1979).

Using this approach, fuselage aerodynamic force is found by

$$\mathbf{F}^b_{A,fuse} = \begin{bmatrix} X_{fuse} \\ Y_{fuse} \\ Z_{fuse} \end{bmatrix} = -\frac{\rho}{2} \begin{bmatrix} X_{fuse,uu}\,|U|\,U \\ Y_{fuse,vv}|V|V \\ Z_{fuse,ww}|W - v_i|(W - v_i) \end{bmatrix}, \tag{8.7-2}$$

where $X_{fuse,uu}$, $Y_{fuse,vv}$, and $Z_{fuse,ww}$ are appropriate dimensional coefficients for each basis function. As formulated, they are the equivalent flat-plate area for flow in each of the three basis directions. Note that the local flow effect of the main rotor, in this case assumed to be located just under the rotor, is approximated. The corresponding moment is estimated by

$$\mathbf{M}^b_{A,fuse} = \begin{bmatrix} L_{fuse} \\ M_{fuse} \\ N_{fuse} \end{bmatrix} = \begin{bmatrix} -z_{fuse} Y_{fuse} \\ -x_{fuse} Z_{fuse} + z_{fuse} X_{fuse} \\ x_{fuse} Y_{fuse} \end{bmatrix}, \tag{8.7-3}$$

where $x_{fuse}$, $z_{fuse}$ is the effective center of the fuselage expressed in the body frame.

This approach applied to a horizontal or vertical tail is just slightly more involved due to the lift generation of these surfaces. Although a conventional Yamaha RMAX does not have a horizontal tail, the equations are included here for completeness and because the Yamaha RMAX configuration documented here had a small horizontal tail added to it (Figure 8.7-1).

The velocity of the vertical tail with respect to the local airflow is approximated by

$$\begin{bmatrix} U^{vt} \\ V^{vt} \\ W^{vt} \end{bmatrix} = \begin{bmatrix} U + Qz_{vt} \\ V + Rx_{vt} - Pz_{vt} + v_{i,tr} \\ W - Qx_{vt} \end{bmatrix}, \tag{8.7-4}$$

where $x_{vt}$, $z_{vt}$ are the effective aerodynamic centers of the vertical tail expressed in the body frame. We have assumed that the vertical tail is close to the tail rotor and entirely within its downwash ($v_{i,tr}$). Only the lateral component of the vertical-tail aerodynamic force is included here,

$$Y_{vt} = -\frac{\rho}{2}(Y_{vt,uv}|U^{vt}|V^{vt} + Y_{vt,vv}|V^{vt}|V^{vt}), \tag{8.7-5}$$

where $Y_{vt,uv}$ acts as the product of the effective lift-curve slope and the area of the vertical tail and $Y_{vt,vv}$ as the equivalent flat-plate area. To account for the potential of the vertical tail exceeding an angle of attack that would result in flow separation, the magnitude of this side force is further limited by

$$Y_{vt,limit} = \pm\frac{\rho}{2}Y_{vt,VV,max}\left(U^{vt2} + V^{vt2} + W^{vt2}\right), \tag{8.7-6}$$

where $Y_{vt,VV,max}$ is effectively the product of the maximum lift coefficient and area of the vertical tail. The aerodynamic side force acting at the vertical tail results in the moment

$$\begin{bmatrix} L_{vt} \\ M_{vt} \\ N_{vt} \end{bmatrix} = \begin{bmatrix} -z_{vt}Y_{vt} \\ 0 \\ x_{vt}Y_{vt} \end{bmatrix} \tag{8.7-7}$$

The horizontal tail is handled in the same manner, with an appropriate change in axes:

$$\begin{bmatrix} U^{ht} \\ V^{ht} \\ W^{ht} \end{bmatrix} = \begin{bmatrix} U + Qz_{ht} \\ V + Rx_{ht} - Pz_{ht} \\ W - Qx_{ht} - v_i \end{bmatrix}, \tag{8.7-8}$$

where $x_{ht}$, $z_{ht}$ are the effective aerodynamic centers of the horizontal tail expressed in the body frame. Here, we assume the horizontal tail is located close to the main rotor and entirely within its downwash ($v_i$). Only the vertical component of the horizontal-tail aerodynamic force is found by

$$Z_{ht} = -\frac{\rho}{2}(Z_{ht,uw}|U^{ht}|W^{ht} + Z_{ht,ww}|W^{ht}|W^{ht}) \tag{8.7-9}$$

Again, we verify this surface does not exceed the force limit

$$Z_{ht,limit} = \pm\frac{\rho}{2}Z_{ht,VV,max}\left(U^{ht2} + V^{ht2} + W^{ht2}\right) \tag{8.7-10}$$

This aerodynamic force component acting at the horizontal tail results in the moment

$$\begin{bmatrix} L_{ht} \\ M_{ht} \\ N_{ht} \end{bmatrix} = \begin{bmatrix} 0 \\ -x_{ht}Z_{ht} \\ 0 \end{bmatrix} \tag{8.7-11}$$

The parameters used to populate this aerodynamic model for the example are included in Table 8.7-5.

**TABLE 8.7-5 Yamaha RMAX Example Model Parameters: Fuselage and Tail**

| Parameter | Value |
|---|---|
| **Fuselage** | |
| $X$-axis force coefficient, $X_{fuse,uu}$ | 2.3 ft$^2$ |
| $Y$-axis force coefficient, $Y_{fuse,vv}$ | 7.8 ft$^2$ |
| $Z$-axis force coefficient, $Y_{fuse,ww}$ | 7.0 ft$^2$ |
| Effective center, body $X$-direction, $x_{fuse}$ | 0 ft |
| Effective center, body $Z$-direction, $z_{fuse}$ | 0 ft |
| **Vertical Tail** | |
| $Y$-axis force coefficient, $Y_{vt,uv}$ | 0.69 ft$^2$ |
| $Y$-axis force coefficient, $Y_{vt,vv}$ | 0.23 ft$^2$ |
| $Y$-axis force coefficient, $Y_{vt,VV,limit}$ | 0.23 ft$^2$ |
| Effective center, body $X$-direction, $x_{vt}$ | −6.2 ft |
| Effective center, body $Z$-direction, $z_{vt}$ | −0.78 ft |
| **Horizontal Tail (not normally included on RMAX)** | |
| $Z$-axis force coefficient, $Z_{ht,uw}$ | 1.9 ft$^2$ |
| $Z$-axis force coefficient, $Z_{ht,ww}$ | 0.63 ft$^2$ |
| $Z$-axis force coefficient, $Z_{ht,VV,limit}$ | 0.63 ft$^2$ |
| Effective center, body $X$-direction, $x_{ht}$ | −2.5 ft |
| Effective center, body $Z$-direction, $z_{ht}$ | −0.59 ft |

## 8.8 SUMMARY

This chapter expanded on the coverage of aerodynamic models for aircraft to include elements necessary to address miniature aircraft. This included coverage of the necessary concepts to understand typical small helicopters, airplanes, and multirotor configurations; computation of the thrust and force of propellers and rotors in hover as well as in forward flight; and modeling of motors and engines typical for small aircraft. There was coverage of the flapping dynamics of helicopter rotors and the use of the stabilizer bar.

Three specific small aircraft examples were provided that make use of the new elements introduced in the chapter.

The first example was the small aerobatic airplane. This airplane is able to transition to hover and act as a "tail sitter" configuration. A model for such a vehicle must address motion in every direction, including sitting still. This necessitated at least approximating the effect of slideslip and angle of attack for their full possible range.

The second example was a multirotor configuration. Here, a typical propeller model becomes a lifting rotor. It was necessary to handle four such rotors for the quadrotor presented. This example utilized electric motors.

The third example, a small unmanned helicopter, added the complexities of a flapping main rotor with a stabilizer bar and a tail rotor as well as the complexities of a transmission, where the modeler must keep track of multiple shaft rates.

## REFERENCES


Abbot, I. H., and A. E. Von Doenhoff. *Theory of Wing Sections*. Mineola, NY: Dover, 1959.

Anderson, J. D. *Introduction to Flight*. New York: McGraw-Hill, 2008.

Chowdhary, G. V., et al. "Integrated Guidance Navigation and Control for a Fully Autonomous Indoor UAS." *Proceedings of the AIAA Guidance, Navigation, and Control Conference*. Washington, D.C.: AIAA, 2011.

Chen, R. T. N., and W. S. Hindson. "Influence of Dynamic Inflow on the Helicopter Vertical Response." *NASA TM 88327*. Washington, D.C.: NASA, 1986.

Dreier, M. E. *Introduction to Helicopter and Tiltrotor Flight Simulation*. Washington, D.C.: AIAA, 2007.

Feldman, J. *DTNSRDC Revised Standard Submarine Equations of Motion*. SPD-0393-09. David W. Taylor Naval Ship Research and Development Center, 1979.

Heffley, R. K., and M. A. Mnich. "Minimum-Complexity Helicopter Simulation Math Model" *NASA CR 177476 (and USAAVSCOM TR 87-A-7),* Washington, D.C.: NASA, 1987.

Heffley, R. K., S. M. Bourne, H. C. Curtis, W. S. Hindson, and R. A. Hess. "Study of Helicopter Roll Control Effectiveness Criteria." *NASA CR 177404 (and USAAVSCOM TR 85-A-5).* Washington, D.C.: NASA, 1986.

Johnson, E.N., and D.P. Schrage. "System Integration and Operation of a Research Unmanned Aerial Vehicle." *AIAA Journal of Aerospace Computing, Information, and Communication,* Washington, D.C.: AIAA, 1, no. 1 (January 2004): 5–18.

Johnson, E. N., M. A. Turbe, A. D. Wu, S. K. Kannan, and J. C. Neidhoefer. "Flight Test Results of Autonomous Fixed-Wing Transition to and from Stationary Hover." *AIAA Journal of Guidance, Control, and Dynamics,* Washington, D.C.: AIAA, Vol. 31, no. 2 (March/April 2008): 358–370.

Leishman, J. G. *Principles of Helicopter Aerodynamics*. Cambridge, U.K.: Cambridge University Press, 2006.

McCormick, B. W. *Aerodynamics of V/STOL Flight*. Mineola, NY: Dover, 1998.

Mettler, B. *Identification Modeling and Characteristics of Miniature Rotorcraft*. Dordrecht, the Netherlands: Kluwer Academic Publishers, 2003.

Perkins, C. D., and R. E. Hage. *Airplane Performance Stability and Control*. New York: Wiley, 1949.

Phillips, W. F. *Mechanics of Flight*. Hoboken, N.J.: Wiley, 2010.

Prouty, R. W. *Helicopter Performance, Stability, and Control*. Malabar, FL: Krieger, 1986.

Simons, M. *Model Aircraft Aerodynamics*. 4th ed., Poole, Dorset, U.K.: Nexus Special Interests, 1999.

Stepniewski, W. Z., and C. N. Keys. *Rotary-Wing Aerodynamics*. Mineola, NY: Dover, 1984.

Stingu, P. E. *Intelligent Control and Cooperation for Mobile Robots*. Ph.D. thesis. University of Texas at Arlington, 2011.


## PROBLEMS

### Section 8.1

**8.1-1** **(a)** Describe the difference between a propeller and a rotor.

**(b)** Describe the difference between an engine and a motor.

**8.1-2** Some multirotor configurations only have three rotors. Describe how they can achieve independent roll, pitch, yaw, and thrust control.

## Section 8.2

**8.2-1** Using the thrust and induced power computations presented in this section, find an exact solution for thrust and power for the special case of hover over a fixed point with no wind.

**8.2-2** The magnitude of the induced velocity of a rotor positively correlates with required power, noise, and (for a VTOL aircraft) kicking up dust and debris when hovering close to the ground. For a given thrust required, what parameter associated with the design of the aircraft do we expect to provide the greatest potential to reduce the induced velocity for a single-rotor helicopter? How about a multirotor?

**8.2-3** A gyrocopter looks similar to a helicopter. It lacks a tail rotor and instead has an engine-driven propeller mounted longitudinally to provide forward thrust. The main rotor is not powered by the engine. For a helicopter, the main rotor disk is tilted forward as it flies. For a gyrocopter, the main rotor is tilted backward as it flies. Explain why this is so.

**8.2-4** Derive Equations (8.2-17) and use them to determine an appropriate linear twist distribution ($\theta_0$ and $\theta_1$) for a 9x7 propeller.

**8.2-5** Having a propeller in the back of an airplane leads to greater directional stability than having the propeller in the front. Estimate the equivalent change to the nondimensional stability derivative associated with directional static stability $C_{n_\beta}$ due to the propeller, accounting for mounting location ($x_p$).

**8.2-6** Some aircraft in the early twentieth century had most of the engine, including all of the cylinders, rotate along with the propeller. This is sometimes called a *rotary* engine. This had a profound effect on the motion of the aircraft when turns were attempted, particularly on these light single-engine aircraft. Identify the source of the phenomenon and provide an estimate of the unexpected moments.

## Section 8.3

**8.3-1** Observe that the first-order tip path dynamics presented in this section do not depend on the number of blades. This implies that one could increase the number of blades (perhaps to increase thrust) and do nothing to the flapping motion. Defend that this is possible. Would a single rotor (with a counterweight) have the same motion as well?

**8.3-2** Using the first-order flapping dynamics for the stabilizer bar presented, derive a corresponding expression for the main rotor flapping angles using the approximation that the main rotor time constant is negligibly small. That is, we treat the main rotor flapping as responding instantly to input.

### Section 8.4

**8.5-1** Estimate the power of a well-designed four-stroke internal combustion engine with 360 cubic inches of displacement running and 2500 RPM at sea level.

**8.5-2** Explain what happens to torque when transferred from one shaft to another where the second is geared to turn twice as fast as the first. Explain what happens to power when going through the same transfer.

### Section 8.5

**8.5-1** Defend the premise that the lift coefficient of a wing with an angle of attack of between 90° and 180° should be less than zero.

**8.5-2** Provide an expression to use for gyroscopic torque to include in this model. Will it be significant?

**8.5-3** Propeller wash over the fuselage can have a twist that leads to moments on the aircraft. Suggest a model change that might approximate the effect, perhaps with an appropriate unknown parameter to be determined by experiment.

### Section 8.6

**8.6-1** Static thrust is the thrust when the aircraft is not moving. Estimate the total static thrust of the aircraft described in this section.

**8.6-2** Some multirotor aircraft have the rotors canted/tilted slightly. The tilt is usually toward the center of the aircraft. Describe what effect this will have if the aircraft has forward speed.

**8.6-3** Suggest a stability augmentation system (SAS) design for this example that utilizes only angular rate feedback. You may consider fixed gain or a dynamic compensator.

### Section 8.7

**8.7-1** The Yamaha RMAX does not normally have a horizontal tail. One was added to an aircraft to hold an antenna and a sensor. Using the parameters provided as well as the methods included in this chapter, estimate the downward force on this surface in a hover.

**8.7-2** Suggest an alternate design for the aircraft without the stabilizer bar and the addition of a stability augmentation system (SAS) that makes the aircraft behave as though it has a stabilizer bar. The emphasis should be on the design of the SAS, not the mechanics of the rotor head.